

Increase in lamin B1 promotes telomere instability by disrupting the shelterin complex in human cells

Gaëlle Pennarun ^{①,2,*†}, Julien Picotto ^{1,2,†}, Laure Etourneau ^{1,2}, Anna-Rita Redavid ^{②,1,2}, Anaïs Certain ^{1,2}, Laurent R. Gauthier ^{1,3}, Paula Fontanilla-Ramirez ^{1,2}, Didier Busso ^{1,4}, Caroline Chabance-Okumura ^{1,2}, Benoît Thézé ^{1,2}, François D. Boussin ^{1,3} and Pascale Bertrand ^{1,2,*}

¹Université de Paris and Université Paris-Saclay, INSERM, iRCM/IBFJ CEA, UMR Stabilité Génétique Cellules Souches et Radiations, F-92265 Fontenay-aux-Roses, France, ²“DNA Repair and Ageing” Team, iRCM/IBFJ, DRF, CEA, Fontenay-aux-Roses, France, ³“Radiopathology” Team, iRCM/IBFJ, DRF, CEA, Fontenay-aux-Roses, France and ⁴Genetic Engineering and Expression Platform (CIGEX), iRCM, DRF, CEA, Fontenay-aux-Roses, France

Received September 15, 2020; Revised August 04, 2021; Editorial Decision August 19, 2021; Accepted August 31, 2021

ABSTRACT

Telomere maintenance is essential to preserve genomic stability and involves telomere-specific proteins, DNA replication and repair proteins. Lamins are key components of the nuclear envelope and play numerous roles, including maintenance of the nuclear integrity, regulation of transcription, and DNA replication. Elevated levels of lamin B1, one of the major lamins, have been observed in some human pathologies and several cancers. Yet, the effect of lamin B1 dysregulation on telomere maintenance remains unknown. Here, we unveil that lamin B1 overexpression drives telomere instability through the disruption of the shelterin complex. Indeed, lamin B1 dysregulation leads to an increase in telomere dysfunction-induced foci, telomeric fusions and telomere losses in human cells. Telomere aberrations were preceded by mislocalizations of TRF2 and its binding partner RAP1. Interestingly, we identified new interactions between lamin B1 and these shelterin proteins, which are strongly enhanced at the nuclear periphery upon lamin B1 overexpression. Importantly, chromosomal fusions induced by lamin B1 in excess were rescued by TRF2 overexpression. These data indicated that lamin B1 overexpression triggers telomere instability through a mislocalization of TRF2. Altogether our results point to lamin B1 as a new interacting partner of TRF2, that is involved in telomere stability.

INTRODUCTION

Telomeres, which constitute the linear ends of eukaryotic chromosomes, are essential for genomic stability and determine the proliferative capacity of cells (1). Dysfunctional telomeres elicit a DNA damage-like response leading to cell cycle arrest, genomic instability, cell death, or senescence depending on cellular context. Mammalian telomeres consist of tandem DNA repeats of the TTAGGG sequence following by a 3' single-strand overhang and adopt a protective T-loop structure formed by the invasion of the 3'-overhang into the telomeric duplex part. This structure hides telomere extremities from being recognized as DNA double-strand breaks by the DNA repair machinery (1). This capped conformation is formed and stabilized by a specialized telomeric protein complex, named ‘shelterin’ (2). Among these proteins, TRF2 plays a key role in the protective function of telomeres. TRF2 binds to the duplex telomeric DNA as a dimer and is required for the T-loop formation by stimulating strand invasion of the 3' overhang into duplex DNA (3–5). Beside its role in t-loop formation, TRF2 can specifically inhibits ATM-dependent DNA damage response signaling as well as NHEJ and HR at telomeres through its interactions with different factors involved in these processes (6–9). Loss of TRF2 function, by expression of a dominant-negative mutant of TRF2 (TRF2^{ΔBΔM}), leads to telomere dysfunction-induced foci (TIFs) (10), end-to-end chromosome fusions, growth arrest and senescence or apoptosis in human cells depending on the genetic background (11–13). RAP1, another shelterin subunit which physically interacts with TRF2, is recruited to telomeres in a TRF2-dependant manner, and thereby reinforces TRF2 affinity for telomeric

*To whom correspondence should be addressed. Tel: +33 1 46 54 98 16; Email: gaelle.pennarun@cea.fr

Correspondence may also be addressed to Pascale Bertrand. Tel: +33 1 46 54 88 46; Email: pascale.bertrand@cea.fr

†The authors wish it to be known that, in their opinion, the first two authors should be regarded as Joint First Authors.

Present address: Anna-Rita Redavid, Apoptosis, Cancer and Development Laboratory- Equipe labellisée ‘La Ligue’, LabEx DEVweCAN, Institut PLAsCAN, Centre de Recherche en Cancérologie de Lyon, INSERM U1052-CNRS UMR5286, Université de Lyon, Centre Léon Bérard, Lyon, France.

sequences (14,15). RAP1 cooperates with TRF2 to protect telomere from recombinations by the homology directed repair pathway (16,17) and from NHEJ (18–20). Recently, RAP1 was found to protect telomeres of human senescent cells (21). In somatic cells, telomere length progressively decreases with aging in part due to end-replication problem, while in tumors cells, telomeres are stabilized by upregulation of the telomerase or by activation of the alternative lengthening of telomeres mechanism (ALT) (22,23). In addition, telomere maintenance in mammalian cells involves numerous other factors principally involved in DNA repair and replication (24,25). Deregulation of these mechanisms plays important role in tumorigenesis and in premature aging. Thus, it is important to identify new factors involved in telomere maintenance and to characterize their interplay with telomeric proteins.

Links between nuclear envelope and telomeres have been well established in the budding yeast in which telomeres aggregate and tether at the nuclear envelope (26). In mammals, meiotic telomeres are attached and clustered to the nuclear envelope and move along during meiotic prophase I (27). While in somatic cells telomeres are localized throughout the cell nucleus (28), they are transitory enriched at the nuclear periphery during post-mitotic nuclear reassembly (29). Telomere tethering to the nuclear envelope during nuclear reassembly was proposed to play a role in the reorganization of chromatin domains in the daughter cells (29). Moreover, a subset of telomeres was also found localized closed to nuclear periphery during replication (30). Interestingly, during senescence of human mesenchymal stem cells, telomeres aggregate and relocate at the lamina (31). Lamins—type V intermediate filament proteins—are major components of the lamina in metazoan organisms, located mainly at the inner layer of the nuclear envelope, and play numerous roles, including maintenance of the nuclear integrity, regulation of chromatin organization, gene expression, DNA replication, DNA damage repair and genome stability (32,33). In mammals, there are two types of lamins: A-type and B-type, that form distinct filamentous meshwork and present with differences in expression pattern, in maturation process or in their protein interaction networks, suggesting that they carry out specific functions (34). A-type lamins expressions are restricted to fully differentiated cells (35), and mutations in lamin A gene have been associated with several degenerative disorders, including muscular dystrophies and premature aging syndrome, as well as the well-known Hutchinson Gilford progeria Syndrome (HGPS) (36,37). B-type lamins are present among all metazoans, including lower organisms and invertebrates, while A-type lamins are restricted to higher organisms with the exception of *Drosophila* that has both types of lamins (38,39). Among lamins, lamin B1 is one of the major lamins, ubiquitously expressed in somatic cells (including undifferentiated cells, differentiated cells and stem cells) from early embryogenesis and throughout life (40). However, a decrease in lamin B1 is observed in senescent cells (41,42). Lamin B1 is permanently farnesylylated, a modification that enables it to be anchored to the inner nuclear membrane, although lamin B1 has been found to form stable structures in nucleus interiors (34,43–46). To date, no human disease has been linked to lamin

B1 loss-of-function or defect, excepted in few tumors including lung carcinoma (47), for which a decrease in lamin B1 has been reported. Very recently, missense mutations in *LMNB1* gene leading to dominant-negative forms of lamin B1 have been involved in primary microcephaly (48,49). Importantly, overexpression of lamin B1 has been seen in few human diseases and in many cancers. Indeed, increased lamin B1 expression due to duplication of the lamin B1 gene (*LMNB1*) causes the rare adult-onset autosomal dominant leukodystrophy (ADLD), a demyelinating neuropathy of the central nervous system (50). Elevated levels of lamins B1 have been also reported in the Werner syndrome (51), and by our team, in the Ataxia-Telangiectasia disorder (AT) and we showed that increased lamin B1 expression accounts for nuclear shape alterations and senescence in this condition (52). More recently, elevated levels of lamin B1 have been found in different types of cancer, including ovary and prostate tumors, as well as, clear cell cancer carcinoma, pancreas and liver cancers (53–59). For these latter three cancers, a positive correlation between lamin B1 expression levels and tumor aggressiveness have been reported (56–58).

However, the mechanisms by which lamin B1 may contribute to tumorigenesis still remain elusive. In order to address this question, we evaluated its impact on chromosome stability especially telomeres. Indeed, telomere dysfunction can favor tumorigenesis (60). Notably telomeric fusions can generate chromosomal instability *via* break-fusion-bridge cycles that lead to genomic rearrangements (61). Previously, it was reported that proliferative defects of fibroblasts induced by lamin B1 overexpression could be rescued by the telomerase catalytic subunit hTERT, suggesting that proliferative defect is associated to telomere alterations/or shortening upon lamin B1 upregulation (62). However, a role of lamin B1 in telomere stability has not been reported yet.

Here, we unveil that lamin B1 is involved in telomere stability. Indeed, we demonstrated that increased level of lamin B1 leads to telomere instability marked by TIFs induction and telomere aberrations, i.e. telomeric fusions and telomere losses. Furthermore, we identified a new interaction between lamin B1 and the key shelterin protein TRF2, as well as with its binding partner RAP1, and that both shelterin proteins are required to form stable complexes with lamin B1. The head-coil domain of lamin B1 and the linker region (or hinge domain (8)) of TRF2 are involved in their association. Thus, lamin B1 is a new interacting partner of mammalian telomere shelterin. We further showed that TRF2 and RAP1 present an aberrant nuclear diffuse localization upon lamin B1 overexpression. These mislocalizations were associated with increased interactions of these proteins with lamin B1, preferentially at the nuclear periphery. Importantly, telomeric instability induced by lamin B1 in excess are counteracted by increasing expression levels of TRF2 protein. Hence, we provide evidences that lamin B1 is a new player in human telomere stability, and propose that its upregulation induces telomere dysfunction and subsequent chromosomal instability through the trapping to nuclear lamina of shelterin proteins, TRF2 and RAP1, leading to aberrant localizations of these latter and impairment of their function.

MATERIALS AND METHODS

Cell cultures

Human cells: normal embryonic diploid fibroblasts, WI-38 (Coriell Cell Repositories), normal primary fibroblasts from healthy donor (GM08399) (Coriell Cell Repositories) and immortalized SV40-fibroblasts (GM0639) (Coriell Cell Repositories) were grown in Dulbecco's modified Eagle's medium (DMEM) medium supplemented with 10% fetal bovine serum (Gibco), 2 mM glutamine and antibiotics (penicillin, 200 U/ml and streptomycin, 200 mg/ml, Sigma) at 37°C with 5% CO₂. Experiments on primary fibroblasts were performed during their proliferative lifespan, up to 15 passages for GM08399 and between 15–22 passages for WI-38, and lack of replicative senescence induction at these passages in basal condition was checked by SA-β-galactosidase assays (data not shown).

Transfection

SV40-fibroblasts were seeded at the density of 1.5 or 1.75 × 10⁵ cells per six-well dishes for most of the experiments or at the density of 1 × 10⁶ cells per 100 mm petri dishes for co-immunoprecipitation) 24 h prior to transfection. For single-transfections, SV40-fibroblasts were transitory transfected using JetPEI (Polyplus) transfection reagent with an empty plasmid as control (CTRL), or a pCMV6 plasmid containing the WT human lamin B1 cDNA (LMNB1). For rescue experiments with TRF2 vectors, SV40-cells were transfected either with empty vector CTRL, LMNB1 vector or a pEGFP plasmid containing human GFP-TRF2-cDNA (GFP-TRF2) or co-transfected with both LMNB1 and GFP-TRF2 vectors with equal number of moles (2.5 × 10⁻¹³ mol of DNA/well). For single transfection, the amounts of plasmids were adjusted with CTRL vector to transfet equal moles of DNA in a ratio 1:1 for each condition. Transient transfection on WI-38 (5 × 10⁵ cells per one transfection in a well of six-well plates using 2 µg of DNA) were performed by nucleofection using Amaxa device (Lonza) following manufacturer's instructions. SiRNAs transfections were performed with Interferin reagent (Polyplus) using 20 nM/well of smart-pool siRNAs designed against lamin B1 (Dharmacon) or a scrambled siRNA as control (Eurogenetec). Efficiency of transfections was checked by western blot or immunofluorescence assays using specific antibodies for proteins of interest.

Constructions of vectors expressing RAP1, TRF2 long isoform, TRF2 linker and lamin B1 fragments

The HA-RAP1 expression vector was obtained by cloning a PCR product (Primer forward: GAAAACCTGTATTTCAGGGCGCTCCGGAA GC GGAGGCGATGGATTG; primer reverse: GGGGACCCTTGTACAAGAAAGCTGGGT CTCGAGTCATTCTTCGAAATTCAATCCTCC) amplified from pCMV6-AC-GFP-RAP1 (RC205112, OriGene) into pDONOR207. Then, the ORF was transferred into pcDNA3-HA puromycin vector by restriction-ligation at the NheI and XhoI sites. The GFP-TRF2 longer isoform expressing vector was purchased from Genscript (Clone

ID OHu16732 into pcDNA3.1 + N-eGFP vector). The linker TRF2 expressing vector (pCDNA-HA-Linker) were obtained by cloning a PCR product (Primer forward: TGAAACAGGCTTCATTTCC; primer reverse: GAAATGAAAGCCTGTTCATATATTGGTTGTA CTGTCATC) amplified from the pEGFPC1-TRF2 vector (kind gift from D. Gomez, IPBS, Toulouse) into pDONOR207. Then, the ORF was transferred into pcDNA3-HA puromycin vector by restriction-ligation at the NheI and XhoI sites. The construction of vectors expressing different Flag-lamin B1 fragments and the Flag-lamin B1 vector were described elsewhere (63). All constructs were verified by DNA sequencing

Immunostaining experiments

For immunostaining of RAP1, TRF1, TRF2 together with lamin B1, cells grown on coverslips, 24 or 48 h after transfection, were pretreated with extraction buffer (50 mM Tris-HCl, 150 mM NaCl, 1% Triton-X100, 1 mM NaF, 1 mM Na₃VO₄, 1 mM PMSF, as described in (64), 2 min on ice before fixation in 2% PFA (10 min)). For single staining with lamin B1, cells were directly fixed in 4% PFA or in ice-cold 100% methanol (10 min). Then, cells were saturated in PBS with 2% BSA-0.05% Tween and stained for 1 h with primary antibodies (mouse anti-TRF1 (Sigma T1348), mouse anti-RAP1 (ab14404, Abcam), mouse anti-TRF2 (Imgenex 124A or Santa Cruz B5) and rabbit anti-lamin B1(ab16048, Abcam), then washed and incubated 1 h with the secondary antibodies (alexa fluor-488 (Life Technologies) or mouse primary antibody and alexa fluor -594 (Life Technologies) for rabbit primary antibody). Nuclei were then counterstained with DAPI and slides were mounted with fluoro-mount mounting medium (Southern Biotech). Images were acquired on epifluorescence microscope leica DM5500B using a 63×-oil objective and analyzed with ImageJ software.

Western-blot

Whole cellular extracts were lysed in SDS buffer (10 mM Tris (pH 7.5), 1% SDS, complete protease inhibitor cocktail (Roche) and phosphatase inhibitors cocktail 2 and 3 (Sigma). 30 to 50 µg of protein extracts were analyzed by SDS-PAGE on a 4–12% NuPAGE Bis-Tris gradient gel or 3–8% Tris-acetate gel and run using MOPS or Tris-acetate running buffer (Invitrogen) following manufacturer's instructions. Gels were transferred on nitrocellulose membrane (Amersham) and immunoblotted using specific primary antibodies: mouse anti-TRF2 (Imgenex 124A or Santa Cruz B5), rabbit anti-lamin B1 (ab16048, Abcam), mouse anti-RAP1 (ab14404, Abcam), lamin A (ab8980, Abcam) and lamin A/C (cs4777, Cell signaling). Rabbit anti-β-actin (2066, Sigma) or mouse anti-Vinculin (ab18058, Abcam) antibodies were used as loading controls. Primary antibodies were either detected using horseradish peroxidase (HRP)-conjugated secondary IgG antibodies (GE Healthcare) and enhanced chemiluminescence detection kit (EZ-ECL, Biological Industries) or using secondary fluorescent antibody (IR800 and IR700, Diagomics). After chemical detection, protein levels were quantified by densitometric analysis of exposed films using ImageJ software.

For near-infrared fluorescent detection, membranes were scanned on Odyssey Imaging system (LI-COR) followed by analysis of protein levels with ImageStudio software (LI-COR). Levels of protein of interest were normalized with respect to loading control.

Metaphase spreading and chromosome analysis

Cells (48 h, 72 h or 6 days after transfection) were plated at the density of 0.5 to 1×10^6 cells per T25-flasks for SV40-fibroblasts or 0.3×10^6 cells per T25 for WI-38. Twenty-four hours after, colcemid (0.1 $\mu\text{g}/\text{ml}$) (Sigma) was added in cell culture medium during the final 2 h. After hypotonic swelling (20 min, 37°C) in prewarmed KCL solution (0.0375M KCl and 1/12 human serum (Lonza) in H₂O), cells were fixed in 3:1 (v/v) ethanol/acetic acid and kept at least 24 h at 4°C. Then cells were washed in fixative solution, dropped onto ice-cold glass slides and aged overnight at room temperature. Then, slides were stained with 4% Giemsa solution (Sigma) and mounted with Eukitt mounting medium. Metaphase spreads were captured using bright-field microscopy (DM5500B, Leica) with a 60 \times -oil objective lens.

Telomere PNA FISH

FISH was carried out following standard procedures (65) on cells grown on coverslips for quantitative-FISH in interphase nuclei (Q-FISH) or on metaphase spreads obtained as described below for quantification of telomeric aberrations. Briefly, slides were rehydrated in PBS and fixed with 4% paraformaldehyde in PBS. After washing, the slides were dehydrated with a cold ethanol series and hybridized with a Cy3-labeled C-rich telomere probe (CCCTAA)₃ with or without a FAM-centromeric PNA probe (Eurogentec) in 70% formamide, 10 mM Tris (pH 7.2), and 1% BSA. DNA was denatured for 3 min at 80°C, and hybridization was carried out at room temperature (RT) in a humidified chamber at least 3 h or overnight. The slides were washed twice in 70% formamide, 10 mM Tris (pH 7.2) and subsequently washed three times in 0.05M Tris (pH 7.2), 0.15 M NaCl and 0.05% Tween-20. Then DNA was counterstained with DAPI and slides were mounted with fluoromount mounting medium and imaging was performed using a SPE Leica laser scanning confocal microscope with a 63 \times -oil objective and analyzed with the ImageJ software. For Q-FISH, quantification was performed with ImageJ software on maximal projection of 3D-images of DAPI, Cya-3 and lamin B1 signals acquired. Nuclei segmentation were performed on DAPI channel and applied to other channels. Cy3-PNA signals (telomere spots) were counted with the local maxima tools or 3D objects counter plugin and the total fluorescence intensity of telomere signals per nucleus was quantified with the 3D objects counter plugin by applying consistent size thresholds. Identical size thresholds were used to compare two experimental conditions. The average DAPI fluorescence intensity for each nucleus was quantified and used to normalize the measured Cy3 PNA fluorescence intensities. The average lamin B1 intensity was quantified for each nucleus. A minimum of 50 nuclei were counted for each condition and experiments were performed in triplicate.

Immuno-FISH

Cells, 48 h after transfection, were fixed with ice-cold 100% methanol or 4% PFA, saturated in PBS with 2% BSA-0.05% Tween and stained for 1 h with primary antibodies (mouse anti- γ -H2AX (Clone JBW301, Milipore) or mouse anti-TRF2 (Imgenex 124A or Santa Cruz B-5) and rabbit anti-lamin B1 (ab16048, Abcam), then washed and incubated 1 h with the secondary antibodies (Alexa fluor-488 (Life Technologies) for mouse primary antibody and Alexa fluor-647 (Life Technologies) for rabbit antibody). Cells were fixed in 2% PFA, dehydrated with ethanol and air dried. Cells were hybridized with the Cy3-labeled C-rich telomere probe (CCCTAA)₃ (Eurogentec) as described for Telomere-FISH. Images were acquired using the SPE confocal microscope and processed with ImageJ software. For TIFs analysis, cells were scored for γ -H2AX foci that colocalized with telomeric PNA signals. For TRF2 immuno-FISH, nuclei were scored for telomere and TRF2 spots co-localization and fluorescence intensity quantification using the ImageJ software. Fluorescent intensities of TRF2 foci localized at telomere were normalized against telomere FISH signal intensity. Telomere intensity per nuclei was normalized to DAPI fluorescent integrated intensity. At least 50 cells were scored for each condition.

Proximity-ligation assay (PLA)

Cells grown on coverslips were fixed in methanol for 10 min, blocked and stained as described above for immunostaining with the following primary antibodies couples: mouse anti-TRF2 (Imgenex 124A) with rabbit anti-lamin B1 (ab16048, Abcam) or mouse anti-RAP1 (ab14404, Abcam) with rabbit anti-lamin B1 (ab16048, Abcam) or mouse anti-HA (HA.11, Biolegend) with rabbit anti-lamin B1 (ab16048, Abcam) or mouse anti-GFP (ab1218, Abcam) with rabbit anti-lamin B1 (ab16048, Abcam) or rabbit anti-Flag (F7425, Sigma) with mouse anti-TRF2 (Santacruz B-5). PLA was performed using the Duolink *in situ* detection Kit (Sigma) according to the manufacturer's protocol. For some experiments, when indicated in figure legends, PLA was coupled with immunostaining of lamin B1 to detect lamin B1-positive cells. For experiments with Flag-lamin B1 constructs or with HA-TRF2-Linker, anti-Flag and anti-HA antibodies, were used to detect Flag or HA expression intensity, respectively. Digital images were acquired with the SPE confocal microscope using a 63 \times -objective lens. Images were processed with ImageJ software.

Co-immunoprecipitation

Cellular proteins from SV40-fibroblasts were extracted on ice using 50 mM Tris-HCl (pH 7.5), 150 mM NaCl, 5 mM EDTA, 0.5% NP40 and a protease inhibitor cocktail (Roche). Protein extracts were treated with the Benzonase nuclease (0.5 U/ μl , E1014, Sigma) supplemented with 10 mM MgCl₂ for 1 h at RT. Dynabeads protein G kit was used for the co-immunoprecipitation (co-IP) according to the manufacturer recommendations (Life Technologies). Briefly, 5 μg of antibodies raised against lamin B1 (ab16048) or TRF2 (Imgenex 124A) were coupled with Dynabeads at RT for 1 h. The beads were subsequently

washed three times with 0.05% Tween-20 in PBS before the incubation step with 0.5–1 mg of protein cell extract (1h30 at RT). Laemmli buffer (2X) with 4% β-mercaptoethanol was used to dissociate and denature the beads-antibodies-proteins complexes. Western blot analysis was performed to reveal the proteins as described above using rabbit anti-lamin B1 antibody (ab16048), mouse anti-TRF2 antibody (Imgenex 124A) or rabbit anti-TRF2 antibody (2645, Cell signaling). As Co-IP controls, aspecific mouse and rabbit IgGs were used (mouse IgG, sc2025 Santa Cruz or rabbit IgG, sc 2027, Santa Cruz).

Statistical analysis

Statistical analyses (unpaired student *t*-tests and Mann-Whitney tests) were performed using GraphPad Prism software.

RESULTS

Lamin B1 overexpression induces telomere instability in human cells

To explore the role of lamin B1 in telomere stability, we decided to focus on the impact of its overexpression on telomere integrity, as main pathological conditions involving lamin B1, i.e. ADLD or several types of cancers, present an upregulation of lamin B1 expression levels. Therefore, we overexpressed lamin B1 in human normal or immortalized fibroblasts. Importantly, the lamin B1 protein levels in overexpressing cells were increased in a range similar to those observed in pathological conditions (Figure 1A and Supplementary Figures S1 and S2A) (1.5- to 5-fold increases in protein levels compared to control conditions such as in ADLD's patient cells (66,67) or in tumor cells with upregulated levels of lamin B1 (54,57,58)). To determine whether lamin B1 upregulation results in telomere dysfunction, we first examined the impact of lamin B1 overexpression on formation of DNA-damage foci localized at telomeres, known as TIFs (telomere-dysfunction induced foci) (10) in immortalized fibroblasts. Immuno-FISH were performed using antibodies against the DNA-damage marker γ-H2AX and lamin B1 (to visualize cells overexpressing lamin B1) and a telomere PNA probe. TIFs, revealed by co-localization between γ-H2AX foci and telomere signal, were dramatically increased by 3.7-fold in cells transfected with lamin B1 compared to control cells, 48 hours after transfection (mean number of 5.6 ± 0.5 TIFs/cells in lamin B1-transfected cells compared to 1.5 ± 0.2 in control cells; $P < 0.0001$) (Figure 1B). Of note, more than 57% of the lamin B1-overexpressing cells were TIFs-positive cells (cells displaying 4 or more colocalizations between telomeric and γ-H2AX signals, as defined in (10) compared to 14.4% in control cells). As alterations in lamin A could also lead to telomere dysfunction (68–70), we checked that, in our experimental conditions, we did not affect the protein levels of other lamins. Indeed, western-blot experiments showed that the protein expression levels of lamin A, as well as lamin B2 and lamin C levels remain unchanged upon lamin B1 overexpression compared to control cells (Supplementary Figure S1). These data thereby indicate that the observed formation of TIFs was due to elevated lamin B1 level and

not indirectly to a potential misregulation of other lamins. Thus, the increase in TIFs indicates that lamin B1 overexpression induces DNA damage at telomeres.

To further characterize the effect of lamin B1 overexpression on telomere stability, we analysed its impact on chromosome stability in metaphase spreads from immortalized fibroblasts. Three days after transfection, we found a significant 2.4-fold increase in chromosome fusion events (i.e. mainly end-to-end-chromosome fusions and at a lower frequency chromatid-type fusions and sister chromatid fusions) in metaphase spreads of cells overexpressing lamin B1 compared to control cells (16.4 ± 2.7 versus 6.9 ± 0.9 fusion events/100 metaphases, $P < 0.0001$) (Figure 1C). These fusion events include telomere fusions as assessed by presence of telomere signals at the fusion points revealed by Telo-FISH (Figure 1D). In lamin B1-overexpressing cells the telomeric fusions were significantly increased by 2.2-fold compared to control cells. These data indicate that lamin B1 overexpression impairs telomere stability in immortalized cells. In association with end-to-end fusions, we also observed by quantitative-FISH a significant decrease in the telomere intensity and in telomeric spot number upon lamin B1 overexpression on interphase nuclei (Figure 1E). Indeed, 3 days after transfection, the telomere intensity per nucleus and the mean telomeric spot number were reduced, respectively, by nearly 40% and 32% in lamin B1-overexpressing cells relative to control cells, suggesting that lamin B1 overexpression leads to telomere losses in human cells. Of note, terminal restriction fragment analysis did not reveal detectable changes in the mean telomere lengths over time upon lamin B1 overexpression compared to control cell population (Supplementary Figure S3), indicating that telomere losses observed by quantitative telomere FISH may correspond to stochastic losses of entire telomere tracts rather than progressive telomere shortening. Moreover, we investigated telomere instability in a doxycycline-inducible stable cell line for lamin B1 overexpression, that exhibits a moderate increase of lamin B1 protein level (2.5-fold compared to control cells, revealed by Western blot analysis) upon doxycycline treatment (Supplementary Figure S4A), as well as in lamin B1 intensity in immunofluorescent staining (2-fold compared to control cells) (Supplementary Figure S4C). A significant increase in fusions events, mainly chromosomal end-to-end fusions, was observed upon induction of lamin B1 overexpression (2.7-fold compared to non-induced control cells) (Supplementary Figure S4D).

As telomere dysfunction can have a differential impact depending on several parameters including cell type and p53 status (71), we checked the impact of lamin B1 overexpression on telomere stability of normal human diploid fibroblasts. These cells exhibit a very moderate expression of lamin B1 (1.5-fold increase compared to control cells) after transfection with lamin B1 vector (Supplementary Figure S2A). Telo-FISH on metaphase spreads, revealed a significant increase in telomere aberrations, mainly telomere losses at one chromatids and telomere fusions of sister chromatids, in lamin B1-overexpressing cells compared to control cells ($P < 0.0001$) (Supplementary Figure S2B). In addition, we observed by Q-FISH, significant decreases in number of telomeric spots and in telomere intensity 7-days after transfection on interphase nuclei of WI-38 cells with a

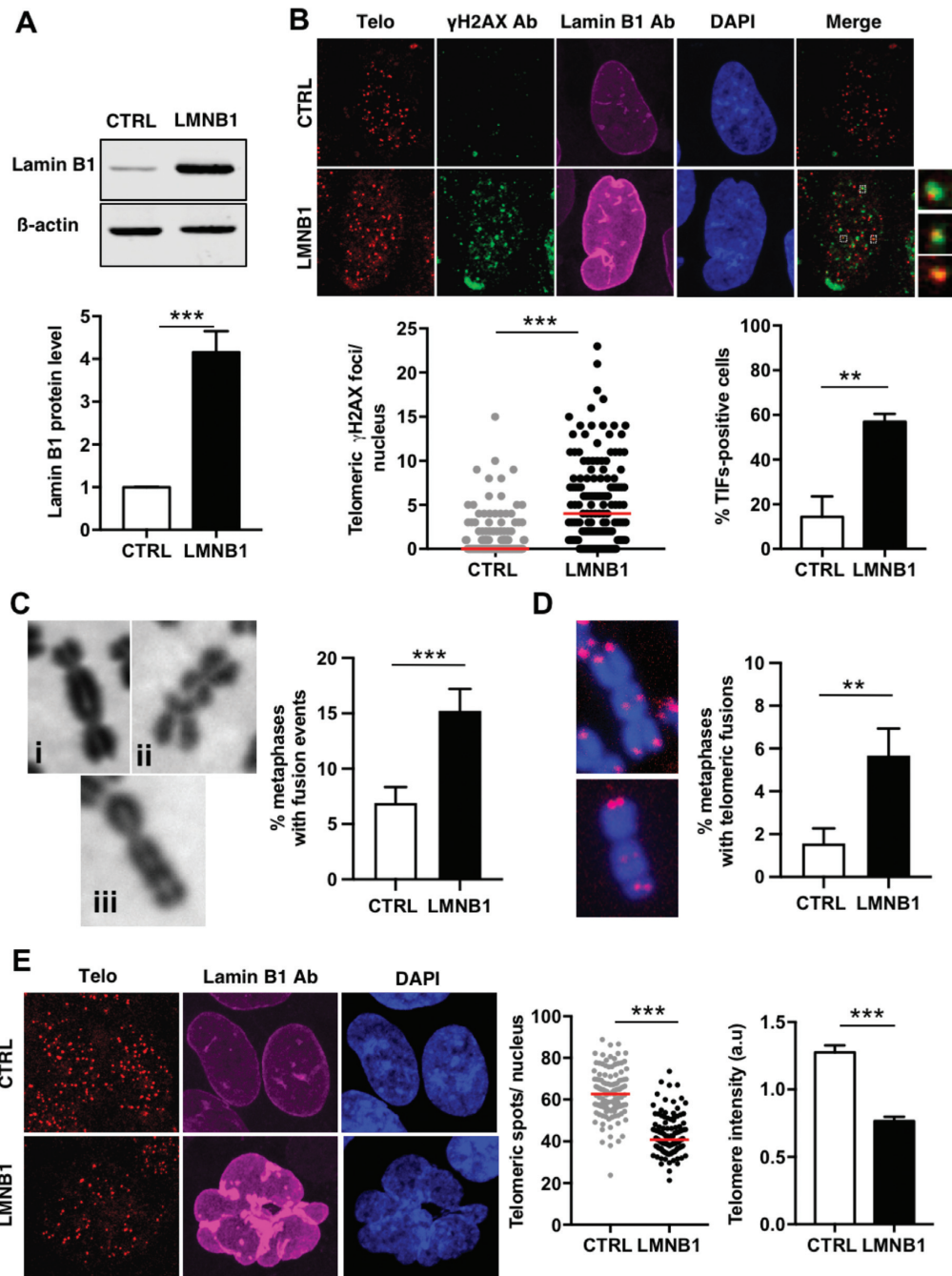


Figure 1. Overexpression of lamin B1 leads to telomere dysfunction in human cells. **(A)** Overexpression of lamin B1 in human immortalized fibroblasts assessed by western blot. 48 h after transfection (either with the empty vector (CTRL) or the lamin B1 vector (LMNB1)), lamin B1 level was controlled by immunoblot using β -actin as loading control. Quantification of lamin B1 protein level from 8 independent experiments is shown (** t -test P value < 0.0001 ; error bars represent SEM). **(B)** Induction of TIFs in lamin B1-overexpressing cells. 48 h after transfection, cells were processed for IF-FISH using a telomeric PNA probe (red) and antibodies against lamin B1 (magenta) and γ -H2AX (green). DNA was counterstained with DAPI. Representative images of IF-FISH from transfected cells are shown on top. Enlarged areas with TIFs are shown on right side. The number of TIFs (γ -H2AX foci colocalized at telomeres) per nucleus (with median values in red) and the percentage of TIFs-positive cells (defined as cells with ≥ 4 TIFs) \pm SD error bars from three independent experiments are shown at the bottom ($n > 120$ cells, *** t -test P value < 0.0001 ; ** $P = 0.0017$). **(C)** End-to-end chromosomal fusions induced 72–96 h after lamin B1 in metaphase spreads from transfected cells with CTRL or LMNB1 vectors. Representative images of chromosomal aberrations found in lamin B1-transfected metaphases stained with Giemsa are shown on left side: chromosome fusions (I), chromatid-type fusions from two chromosomes (II) and sister chromatid fusions (III). Quantification of fusion events (means \pm SEM) is shown at the right. A minimum of 354 metaphases, from four independent experiments, were analyzed for each condition (** t -test P value < 0.0007). **(D)** Telomere fusions (fusion with telomere signals at the junction point) identified by TelofISH on metaphase spreads from cells described in (C). Representative images of telomere fusions and their quantification (means \pm SEM) are shown. A minimum of 264 metaphases from four independent experiments were analyzed for each condition (** t -test P value = 0.0053). **(E)** Telomere loss upon lamin B1 overexpression by Q-FISH analysis performed on interphase nuclei of transfected cells (CTRL or LMNB1), 72 h after transfection. Representative images are shown. The mean numbers of telomere spot signals per nucleus (with median values in red) and total fluorescence intensity of telomere signals per nucleus (means \pm SEM) are shown (from $n = 3$ independent experiments; *** t -test P value < 0.0001).

modest overexpression of lamin B1 ($P < 0.0001$ and $P = 0.0055$, respectively) (Supplementary Figure S2C). These data indicate that lamin B1 overexpression compromises telomere integrity in both transformed human fibroblasts and normal fibroblasts, even at low levels of overexpression (1.5-fold) (Supplementary Figure S2A). Therefore, these data unveil that in human cells, lamin B1 overexpression leads to telomere instability marked by TIFs and telomeric aberrations, i.e. telomeric fusions and telomere losses.

The shelterin proteins TRF2 and RAP1 are delocalized upon lamin B1 overexpression

To explore the events that could initiate telomere instability upon lamin B1 overexpression, we investigated the impact of lamin B1 upregulation on the key shelterin protein TRF2, as its defect leads to telomere decapping and subsequent TIFs and telomere instability (10,13). We first analyzed the localization of this shelterin protein, upon lamin B1 overexpression by immunofluorescent staining. Confocal microscopy reveals that increased levels of lamin B1 lead to a rapid mislocalization of TRF2 in nearly $43.2\% \pm 4.6$ of the total lamin B1-overexpressing cells at 24 h, and up to $68.2\% \pm 5.7$ at 48 h compared to, respectively, $10\% \pm 3.9$ and $19.5\% \pm 4.5$ in control cells (Figure 2A). Indeed, TRF2 displays a typical punctate staining pattern in normal control cells (4), while lamin B1-overexpressing cells have an aberrant pattern of TRF2, i.e. disappearance of TRF2 foci leading to a diffuse staining in the nucleus (Figure 2A). Importantly, delocalization of TRF2 occurs even at a low level of lamin B1 overexpression (2–5-fold, similar to pathological conditions with upregulation of lamin B1) as shown in Figure 2A ($77.8\% \pm 6.3$ in 2–5-fold overexpressing lamin B1 cells at 24 h) and by the analysis of correlation between TRF2 foci number and lamin B1 level in nuclei (Supplementary Figure S5). Quantitative analysis revealed that the total mean fluorescence intensity of TRF2 per nucleus remains statistically identical between control and lamin B1 overexpressing cells (Figure 2B), while the number of TRF2 foci was decreased significantly (Supplementary Figure S5B). In addition, we showed by western blot that TRF2 protein level did not decrease upon lamin B1 overexpression (Figure 2C), suggesting that loss of typical TRF2 punctuate pattern is not due to a degradation of TRF2 protein but rather to a re- or delocalization of the protein. Furthermore, mislocalization of TRF2 upon lamin B1 overexpression was confirmed in normal embryonic fibroblasts WI-38 (Supplementary Figure S2D) and in the inducible cell line for lamin B1 overexpression (Supplementary Figure S4C). To further analyze whether TRF2 was delocalized from telomeres, immunolocalization of endogenous TRF2 with telomeres detected by FISH in lamin B1-overexpressing cells was analyzed by confocal microscopy, 48 h after transfection. While almost all telomeres were colocalized with TRF2 foci in control cells (as determined by the overlap between both TRF2 and telomere signals in fluorescent intensity profiles, Figure 2D), numerous telomere signals were devoid of TRF2 foci in lamin B1-overexpressing cells, as shown by lack of TRF2 signal colocalized at telomere signal peaks. In particular, immunofISH quantifications show that there were almost 4-fold

more telomeres completely devoid of TRF2 foci in lamin B1-overexpressing cell compared to control cells ($28.9\% \pm 2.7$ compared to $7.4\% \pm 1.0$), in association with a significant decrease in TRF2 fluorescent intensity at telomeres (53%), while the average telomere spots intensity per cells remained similar in both conditions (Figure 2E). Notably, the telomere localization was not affected 48 and 72 h after lamin B1 overexpression as assessed by the percentage of telomere signals in the nuclear periphery area that is similar in CTRL and lamin B1-overexpressing cells (Supplementary Figure S6). These data indicate that the disappearance of TRF2 foci localized at telomeres precedes telomere losses observed in lamin B1-overexpressing cells, suggesting that TRF2 may be delocalized from telomere upon lamin B1 overexpression. To confirm this kinetic of events, we analyzed the induction of telomere losses and fusion events, 24, 48 and 72 h after lamin B1-transfection. The earliest detection of significant induction of telomere losses and fusion events was 72 h after lamin B1 overexpression, while no significant increase of these aberrations was detected 24 or 48 h following lamin B1-transfection (Supplementary Figure S7A and B). Thus, our data showed that the mislocalization of TRF2 upon lamin B1 overexpression occurs quickly (24 h after transfection (Figure 2A)) during the first cell cycle, suggesting that cell divisions are not needed for this event. As the induction of telomeric instability (i.e. telomeric fusions and losses) were observed upon two or three subsequent cell divisions (72 h after transfection (Supplementary Figure S7A and B)), our data indicate that TRF2 delocalization is not a consequence of telomere losses but rather the initial event of telomere instability.

To further characterize whether lamin B1 overexpression induces telomere uncapping, we also investigated its impact on the localization of other shelterin proteins. Immunofluorescent staining of TRF2's binding partner RAP1 showed that overexpression of lamin B1 also affects its localization inside the nucleus (i.e. disappearance of the typical focal staining pattern of RAP1 (14) in $76.5\% \pm 2.9$ of the lamin B1-overexpressing cells compared to $4.4\% \pm 1.3$ in control cells), even at low level of lamin B1-overexpression (1–5-fold), without affecting the protein level of RAP1 (Figure 3A and B). Since the localization of RAP1 at telomeres requires TRF2 binding to telomeric DNA (14), the abnormal RAP1 staining is consistent with the defect of TRF2 recruitment to telomeres. By contrast, the percentage of cells with abnormal staining pattern of TRF1, as well as the mean number of TRF1 foci per nucleus, were not significantly increased upon lamin B1 overexpression compared to that observed in control cells (Figure 3C). These data suggest that lamin B1 overexpression first affects the telomeric cap rather than the whole telomere tract. Altogether our data indicate that lamin B1 overexpression may induce telomere uncapping and subsequent telomere instability by altering localization of TRF2 and RAP1.

Lamin B1 interacts endogenously with TRF2 and RAP1 and these associations are enhanced at the nuclear periphery upon lamin B1 overexpression

The mislocalization of both TRF2 and RAP1 upon lamin B1 overexpression raises the possibility that lamin B1 may interact with these key shelterin proteins. We first investi-

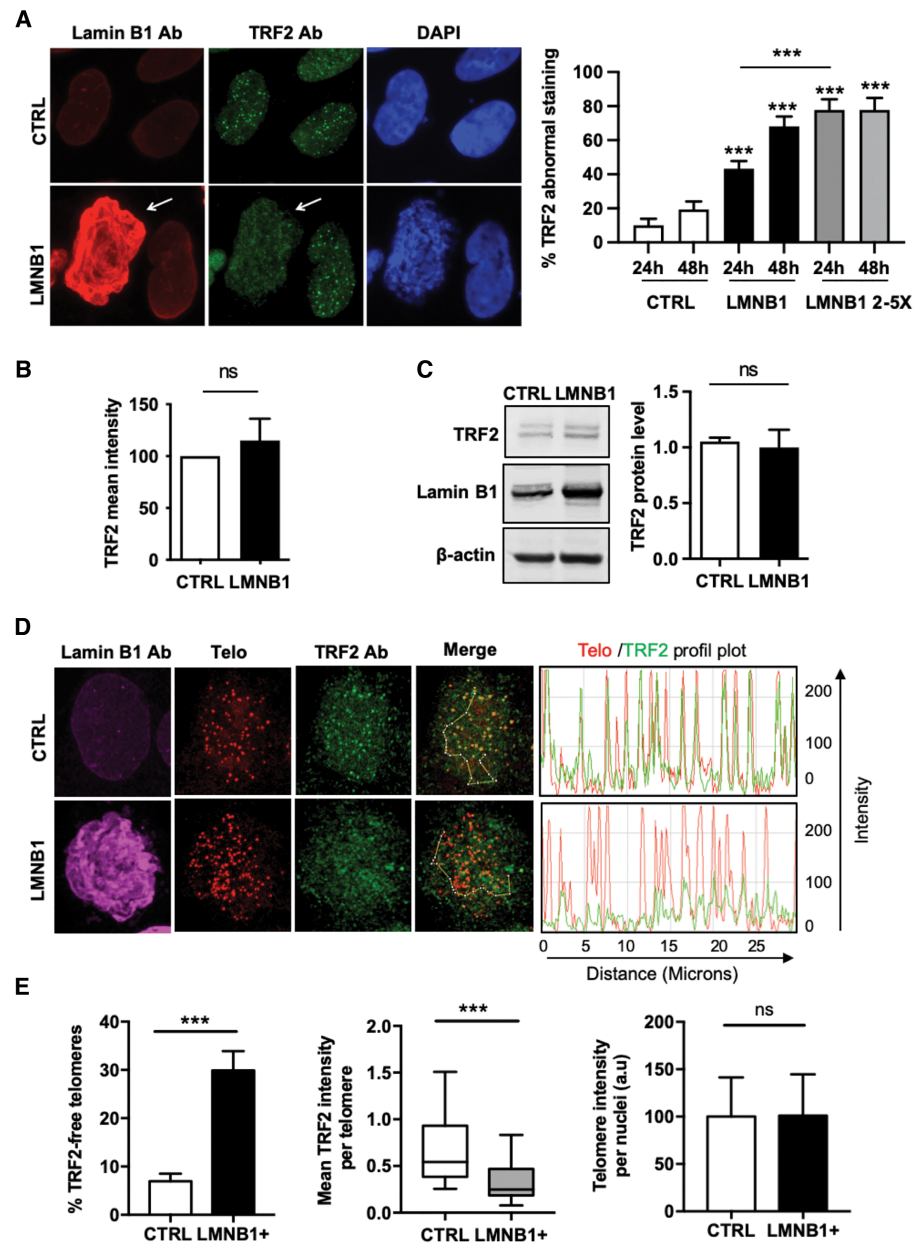


Figure 2. Delocalization of the shelterin protein TRF2 after lamin B1 overexpression (A) Indirect immunofluorescence analysis of TRF2 in human SV40-fibroblasts, 24 and 48 h after transfection with CTRL or LMNB1 expression vectors. Representative images are shown on the left: cells were immunostained with antibodies specific for TRF2 (green) and lamin B1 (red) and nuclei were counterstained with DAPI. Arrows point a cell nucleus overexpressing lamin B1 in association with altered TRF2 staining pattern. Percentages of cells with abnormal TRF2 staining are shown in cells transfected with control vector (CTRL) or with lamin B1 vector, divided in two categories: total population of lamin B1 overexpressing cells (LMNB1) or 2–5 fold overexpressing cells as in a pathological range (LMNB1 2–5×) (means ± SEM of two independent experiments are shown (***) *t*-tests *P* value < 0.0001 between CTRL and LMNB1 for the different time point 24 and 48 h, *P* < 0.0001 between LMNB1 2–5× and total LMNB1 at 24 h). (B) Indirect immunofluorescence analysis of TRF2 in human SV40-fibroblasts, 48 h after transfection with CTRL or LMNB1 expression vectors. Quantification of TRF2 mean fluorescent intensity per nuclei in transfected cells compared with control cells is shown (histograms show means ± SD from three independent experiments) (ns = *t*-test *P* value non-significant). (C) Western-blot analysis of TRF2 protein levels 48 h after transfection in cells described in (A). Cell lysates were processed for western blotting with antibodies specific for TRF2, lamin B1 and β-actin as loading control. Representative blots and quantification from 7 independent experiments are shown (right panel) (histograms show means ± SEM; ns = *t*-test *P* value non-significant). (D, E) TRF2 is delocalized from telomere upon lamin B1 overexpression. (D) Representative confocal microscopic images of immuno-FISH performed with telomere PNA probe (red) and specific antibodies against TRF2 (green) and lamin B1 (magenta) from cells 48 h after transfection with CTRL or LMNB1 vectors. White lines on merge images correspond to the path used for fluorescent intensity profiles analysis with ImageJ. On right side, fluorescent intensity profiles showing colocalizations of TRF2 and telomere signals in CTRL (top) or LMNB1-overexpressing cells (bottom). (E) Left panel, quantification of the percentages of telomeres devoid of TRF2 foci in control cells (CTRL) or lamin B1-positive cells (with an average 3-fold overexpression). Histogram shows the mean (± SEM) from two independent experiments (*n* = 50 cells analyzed per condition, ****P* < 0.0001). Middle panel, quantification of TRF2 fluorescent intensity at telomere per nucleus normalized against telomere FISH signal intensity in the same cells analyzed for the left panel and compiled in a Tukey box plot (***Mann-Whitney test *P* value < 0.0001). Right panel, quantification of telomere intensity per nuclei normalized to DAPI intensity is shown. Graph represents mean (± SD) in the same cells analyzed for the left and middle panels (*t*-test *P* value ns = non-significant).

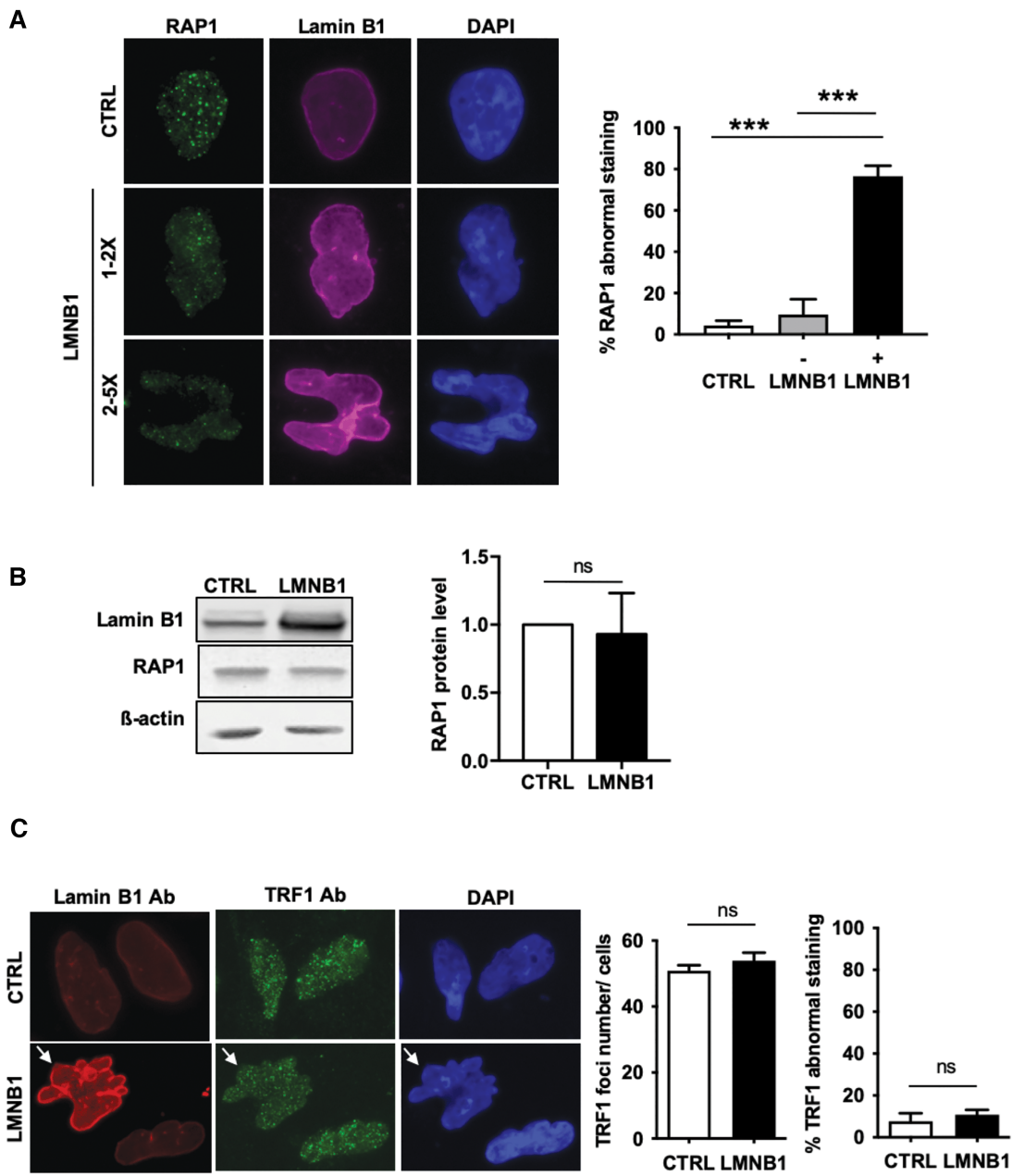


Figure 3. Delocalization of the shelterin TRF2-interacting partner RAP1 but not TRF1 after lamin B1 overexpression (A) Indirect immunofluorescence analysis of RAP1 in SV40-fibroblasts 48 h after transfection with CTRL or LMNB1 expression vectors. Representative images of cells overexpressing lamin B1 by 1-fold and 2-fold are shown on the left panel: cells were immunostained with antibodies specific for RAP1 (green) and lamin B1 (red) and nuclei were counterstained with DAPI. Percentages of cells with abnormal RAP1 staining are shown on the right panel in cells transfected with control vector (CTRL) or with lamin B1 vector (LMNB1), divided in two categories (cells overexpressing lamin B1 (+) or with no significant overexpression of lamin B1 compared to control (-)). Means \pm SD of three independent experiments. *** t -test P value < 0.0002 . (B) Western-blot analysis of RAP1 protein levels in cells described in (A). Cell lysates were processed for western blotting with antibodies specific for RAP1, lamin B1 and β -actin as loading control. Representative blots and quantification from six independent experiments are shown (right panel). Histograms show means \pm SD; ns = t -test P value non-significant. (C) Indirect immunofluorescence staining of TRF1 in SV40-fibroblasts 48 h after lamin-B1 overexpression. Representative images are shown on top: cells were immunostained with antibodies specific for TRF1 (green) and lamin B1 (red) and nuclei were counterstained with DAPI. At bottom, quantification of TRF1 foci number per cells is shown on left from three independent experiments (means \pm SEM; ns = t -test P value non-significant). Quantification of cells with abnormal staining pattern of TRF1, 48 h after lamin B1-overexpression, is shown on right (mean \pm SEM from three independent experiments; ns = t -test P value non-significant)

gate whether lamin B1 could interact with TRF2 in human fibroblasts by *in situ* proximity ligation assay (PLA) staining. Using a couple of specific antibodies against these two proteins, we showed a new interaction in close proximity between endogenous TRF2 and lamin B1 in human cells, as shown by the formation of red dots. The PLA dots number is significantly reduced by nearly 3-fold with siRNA against lamin B1, showing the specificity of the interaction (Figure 4A). Moreover, we confirmed endogenous TRF2-lamin B1 interactions in two other cell types: normal diploid embryonic fibroblasts WI-38 and normal adult primary fibroblasts (Figure 4B). Of note, the endogenous TRF2-lamin B1 interactions are localized throughout the nucleus, and not particularly at the nuclear periphery. In accordance with these observations, previous papers have reported a pool of lamin B1, not associated with lamina, in the nucleoplasm, forming stable structures detectable as discrete foci (34,43,46), suggesting that the endogenous interactions between TRF2 and lamin B1 also involve nucleoplasmic lamin B1. We next evaluated the impact of lamin B1 overexpression on TRF2-lamin B1 interaction. We performed *in situ* PLA assay coupling with lamin B1 staining on immortalized fibroblasts transfected by lamin B1-expression vector or empty-control vector and found that signal dots of TRF2-lamin B1 PLA were increased by 2.6-fold and 5-fold for a 1–2-fold and 2–5-fold lamin B1-overexpression, respectively ($P < 0.0001$) (Figure 4C). Importantly, increase in lamin B1-TRF2 PLA dots was detected as early as 24 h after transfection in kinetic experiments upon lamin B1 overexpression, even at low lamin B1 level of overexpression (2–5-fold) (Supplementary Figure S7C). We also confirmed the increase in TRF2-lamin B1 PLA dots upon moderate lamin B1 overexpression in the inducible cell line for lamin B1 treated with doxycycline (Supplementary Figure S4B). Interestingly, the localization of the interacting dots was significantly enriched at the nuclear periphery, as shown by the 3D-confocal image analysis ($70.8\% \pm 2.3$ of dots in the area of nuclear periphery for lamin B1-overexpressing cells compared to 33% for control cells, equivalent to the value for a random distribution of dots in the nucleus (29)) (Figure 4D). To better visualize the accumulation of PLA dots at the nuclear periphery, we performed PLA coupled with staining of emerin, a nuclear protein localized at the inner nuclear membrane (72). This co-staining enables us to visualize concomitant localization of lamin B1-TRF2 PLA interaction at the nuclear rim (Supplementary Figure S8). Furthermore, we found a new interaction between endogenous RAP1 and lamin B1 proteins by *in situ* PLA staining (Figure 5A). We showed that this interaction was also significantly increased by 5.1-fold upon lamin B1-overexpression (Figure 5C) and preferentially enriched at the nuclear periphery (Figure 5D).

We further confirmed the TRF2-lamin B1 interaction by using co-immunoprecipitation experiments. Indeed, immunoprecipitation of endogenous TRF2 protein from lysates of lamin B1-overexpressing cells, revealed co-precipitation of lamin B1 (Figure 4E). In endogenous conditions, a weak signal for endogenous lamin B1 was detected in pull-down experiment with an antibody specific to TRF2, indicating that both TRF2 and lamin B1 could also interact endogenously, confirming their endogenous associ-

ation observed in PLA experiments. Of note, since lamin B1 and TRF2 have been reported to have the ability to directly bind DNA (4,73), we pre-treated cell lysates with a nuclease prior to co-immunoprecipitation experiments to rule out the possibility that the two proteins co-precipitate through DNA-bridging. These experiments indicate that lamin B1 and TRF2 can be found in a common protein complex independently of DNA at a weak level in endogenous conditions and much more robustly upon lamin B1 overexpression. In addition, we confirmed the interaction of RAP1 with lamin B1 by co-immunoprecipitation from cellular lysates pre-treated with benzonase, indicating that this interaction may occur independently from DNA (Figure 5B). Interestingly, the interaction between TRF2 and lamin B1 is affected by RAP1 depletion, and reciprocally, TRF2 inhibition leads to a decrease in lamin B1-RAP1 interaction (Figure 5E and F). These data showed that both RAP1 and TRF2 may play a role in the stabilization of the interaction of lamin B1 with their shelterin partner, and that lamin B1 may form a common complex with both RAP1 and TRF2.

Taken together our data unveil a new interaction between endogenous lamin B1 and TRF2 proteins, and we further showed that this interaction is significantly enhanced and preferentially enriched at the nuclear periphery upon lamin B1 overexpression. We also found a new interaction between endogenous lamin B1 and RAP1, that is also significantly enhanced especially at the nuclear periphery with increased lamin B1 level, suggesting that lamin B1 overexpression leads to a deprotection of telomeres by trapping TRF2 and RAP1 outside from telomeres.

The N-terminal-coil1 region of lamin B1 and the linker region of TRF2 are involved in their associations

We next characterized the interaction between shelterin TRF2 and lamin B1 by using different constructions of these proteins (Figure 6A). A longer isoform of TRF2 protein has been recently characterized, with an additional N-terminal extension of 42 aminoacids upstream of the previously identified start codon (74), that shares similar role as the first isoform reported of TRF2 in telomere protection and t-loop formation. By co-immunoprecipitation with protein extracts from cells transfected with an expression vector of the GFP-tagged longer TRF2 isoform, we showed that endogenous lamin B1 co-immunoprecipitates also with this longer isoform (Figure 6B). We further confirmed the interaction of endogenous lamin B1 with the TRF2 longer isoform by PLA assay (Figure 6C). Very recently, the linker region of TRF2 (also referred as the Hinge domain (8), located between the TRFH and Myb domains, has been reported to interact with lamins, including lamin B1, by co-immunoprecipitation from enriched nuclear lamina extracts (75). In accordance with this paper, by PLA assay, we found that the linker region interacts with the endogenous lamin B1 protein *in situ* in cells transfected with a vector expressing the TRF2 linker fragment (Figure 6D). To further characterize which domain(s) of lamin B1 could be involved in its interaction with the shelterin TRF2, we expressed vectors coding for different domains of lamin B1 and analyzed their interaction with TRF2 by PLA (Figure 6A). Interestingly, we found a high interaction with TRF2 in cells trans-

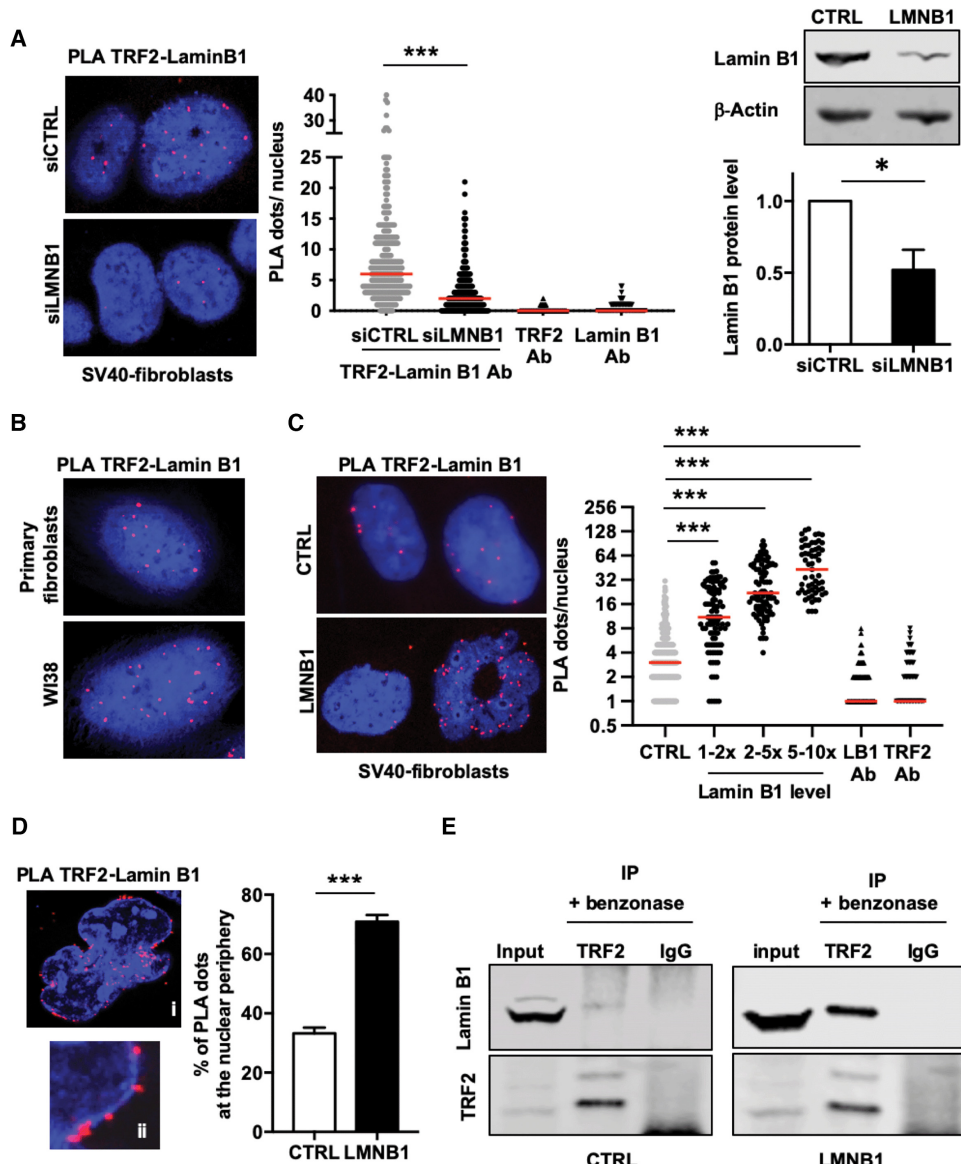


Figure 4. Lamin B1 interacts with TRF2 and its overexpression enhances their association preferentially at the nuclear periphery (A) SV40-fibroblasts transfected either with siRNA targeting lamin B1 (siLMNB1) or control siRNA (siCTRL) for 48 h were processed for lamin B1-TRF2 PLA using specific antibodies against these proteins. *Left*, representative confocal images of PLA experiments showing *in situ* interaction between TRF2 and lamin B1 visualized as red fluorescent dots in nucleus delimited by DAPI counterstaining (blue). *Middle*, quantification of PLA dots per nucleus (medians are shown in red; $n = 3$ independent experiments; ≥ 249 nuclei analyzed per siCTRL or siLMNB1 condition; *** t -test P value < 0.0001). PLA was also performed using one of the primary antibody against TRF2 or lamin B1 protein alone as a negative control (TRF2 Ab or Lamin B1 Ab). *Right*, Western-blots analysis of lamin B1 protein levels from cells described in (A), 48 h after transfection, showing partial inhibition of lamin B1. Hybridizations were performed with a specific antibody against lamin B1 (upper panel) and β-actin (lower panel) antibody, used as loading control. Quantification from three independent experiments is shown (* t -test P value < 0.01). (B) Representative PLA images showing *in situ* interaction between Lamin B1 and the telomeric protein TRF2 in normal human adult and embryonic primary fibroblasts (GM08399 and WI-38, respectively). Cells were subjected to proximity ligation assay (PLA) using antibodies against lamin B1 and TRF2. Similar results were obtained in two independent experiments. (C) TRF2-Lamin B1 interaction as a function of lamin B1 intensity monitored by PLA coupled with lamin B1 immunofluorescent staining. Level of lamin B1 overexpression was categorized in three classes as a fold increase compared to endogenous level: 1- to 2-fold, 2- to 5-fold or 5- to 10-fold (respectively Intensity categories: 1–2x, 2–5x, 5–10x). Quantification of TRF2-lamin B1 dots per nuclei show a significant increase even at low doses of lamin B1 overexpression (2–5-fold) compared to control cells (medians are shown in red, *** t -test P value < 0.0001 ; $n = 3$ independent experiments); PLA negative controls with only one of the antibodies against TRF2 or lamin B1 are shown (TRF2 Ab or LB1 Ab). (D) Quantification of the percentage of TRF2-lamin B1 PLA signals per nuclei that were localized in the area of the nuclear envelope in Z-stacks from 3D confocal images obtained from PLA experiments on lamin B1-overexpressing cells (LMNB1+) compared to control cells as described in (C). Histogram shows the mean \pm SD from three independent experiments ($n \geq 65$ nuclei analyzed per condition, t -test P value < 0.0001). On the left side (i), nucleus from LMNB1-transfected cell with TRF2-lamin B1 PLA signals (in red) and DAPI staining (in blue) and an enlargement (ii) of an area of the nucleus showing PLA dots (in red) localized at the nuclear periphery. (E) Immunoprecipitation of endogenous TRF2 revealed pull-down of lamin B1 in endogenous conditions (CTRL) and upon lamin B1 overexpression (LMNB1). SV40-fibroblasts were transfected with lamin B1 expression vector (LMNB1) or control vector (CTRL) and after 48 h, lysates, pretreated with benzonase nuclease, were immunoprecipitated with anti-TRF2 antibody or anti-IgG antibody as control and analyzed by western-blots with antibodies specific to TRF2 and lamin B1. Similar results were obtained in three independent experiments.

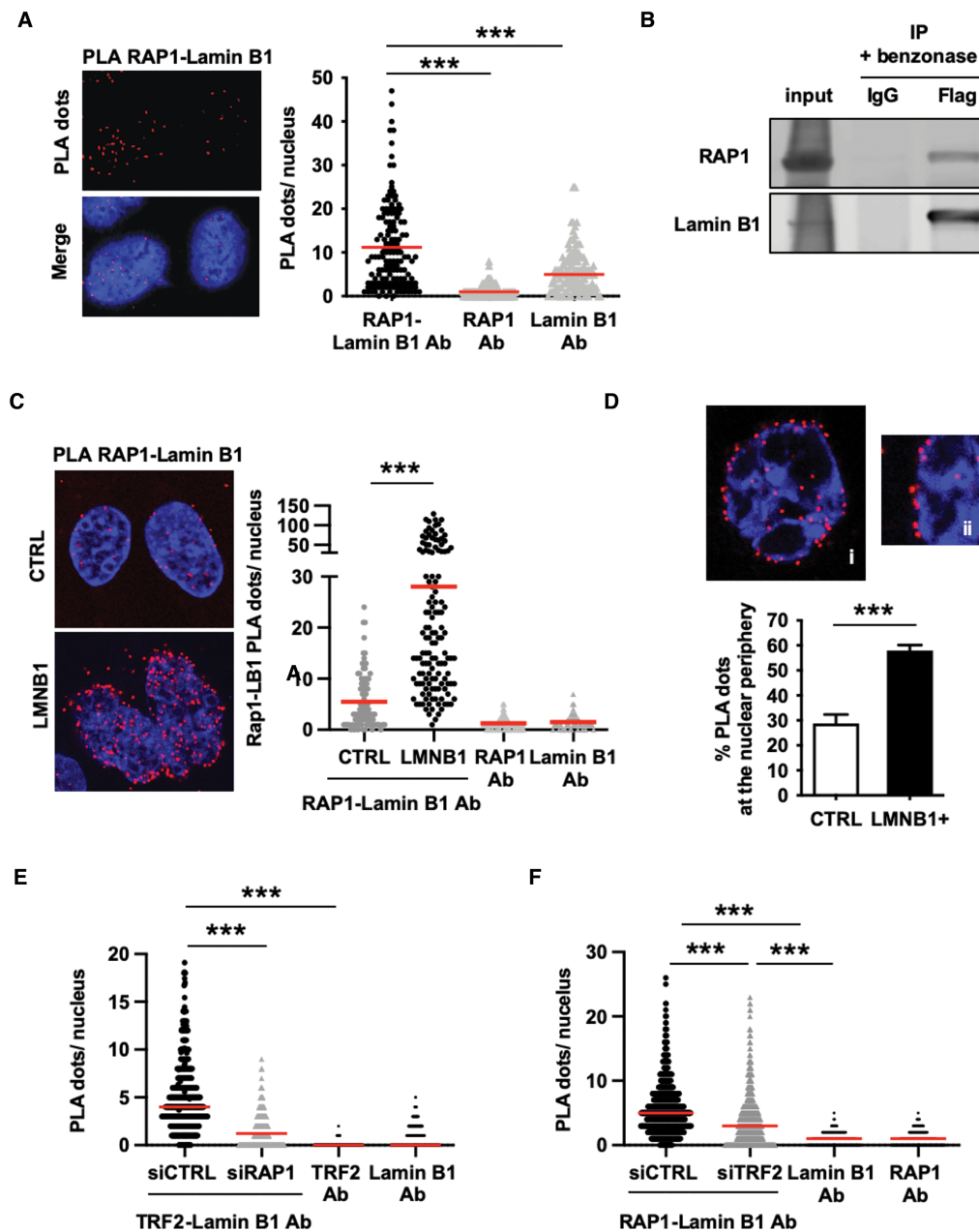


Figure 5. Lamin B1 interacts endogenously with RAP1 and its overexpression enhances their association preferentially at the nuclear periphery (A) SV40-fibroblasts were subjected to proximity ligation assay (PLA) using antibodies against lamin B1 and RAP1. Right, representative confocal images showing *in situ* interaction between lamin B1 and RAP1 visualized as red fluorescent dots in nucleus delimited by DAPI counterstaining (blue). Left, quantification of RAP1-Lamin B1 PLA dots per nucleus (medians in red; $n = 3$ independent experiments; ≥ 129 nuclei per condition; *** t -test P value < 0.0001). PLA was also performed using one of the primary antibody against RAP1 or lamin B1 protein alone as a negative control (RAP1 Ab or Lamin B1 Ab). (B) Co-immunoprecipitation (co-IP) of lamin B1 and RAP1. SV40-fibroblasts were co-transfected with FLAG-Lamin B1 and HA-RAP1 expressing vectors and co-IP was carried out using anti-flag antibody on cellular lysates—pretreated with benzonase—and analyzed by Western blot using specific antibodies against lamin B1 or RAP1 protein. Similar results were found in two independent experiments. (C) Quantification of RAP1-Lamin B1 PLA dots in SV40-fibroblasts transfected either with lamin B1-expressing vector (LMNB1) or control vector (CTRL) and subjected to PLA as described in (A), 48 h after transfection. Data combined from 2 independent experiments are shown (means in red; ≥ 92 nuclei per condition; P value < 0.0001) (D) Quantification of the percentage of RAP1-lamin B1 PLA signals per nuclei that were localized in the area of the nuclear envelope in Z-stacks from 3D confocal images obtained from PLA experiments on lamin B1-overexpressing cells (LMNB1+) compared to control cells (mean \pm SEM from $n \geq 50$ nuclei analyzed per condition is shown; t -test P value < 0.0001). Similar results were obtained in three other independent experiments. On the left side (i), nucleus from LMNB1-transfected cell with RAP1-lamin B1 PLA signals (in red) and DAPI staining (in blue) and an enlargement (ii) of an area of the nucleus showing PLA dots (in red) localized at the nuclear periphery. (E, F) Impact of RAP1 depletion on TRF2-lamin B1 interaction and reciprocally, impact of TRF2 depletion on RAP1-lamin B1 interaction. SV40-fibroblasts transfected either with siRNA targeting RAP1 (siRAP1), TRF2 (siTRF2) or control siRNA (siCTRL) for 48 h were processed for lamin B1-TRF2 PLA (E) or lamin B1-RAP1 PLA (F) with specific antibodies (Ab) or one antibody alone as control. Quantification of PLA dots per nucleus (medians are in red; $n > 100$ nuclei per conditions per experiment; *** t -test P value < 0.0001 , $n = 4$ and $n = 6$ independent experiments for panels (E) and (F), respectively). Negative PLA controls performed with one of the primary antibody against RAP1, TRF2 or lamin B1 protein alone (RAP1 Ab, TRF2 Ab or Lamin B1 Ab) are shown.

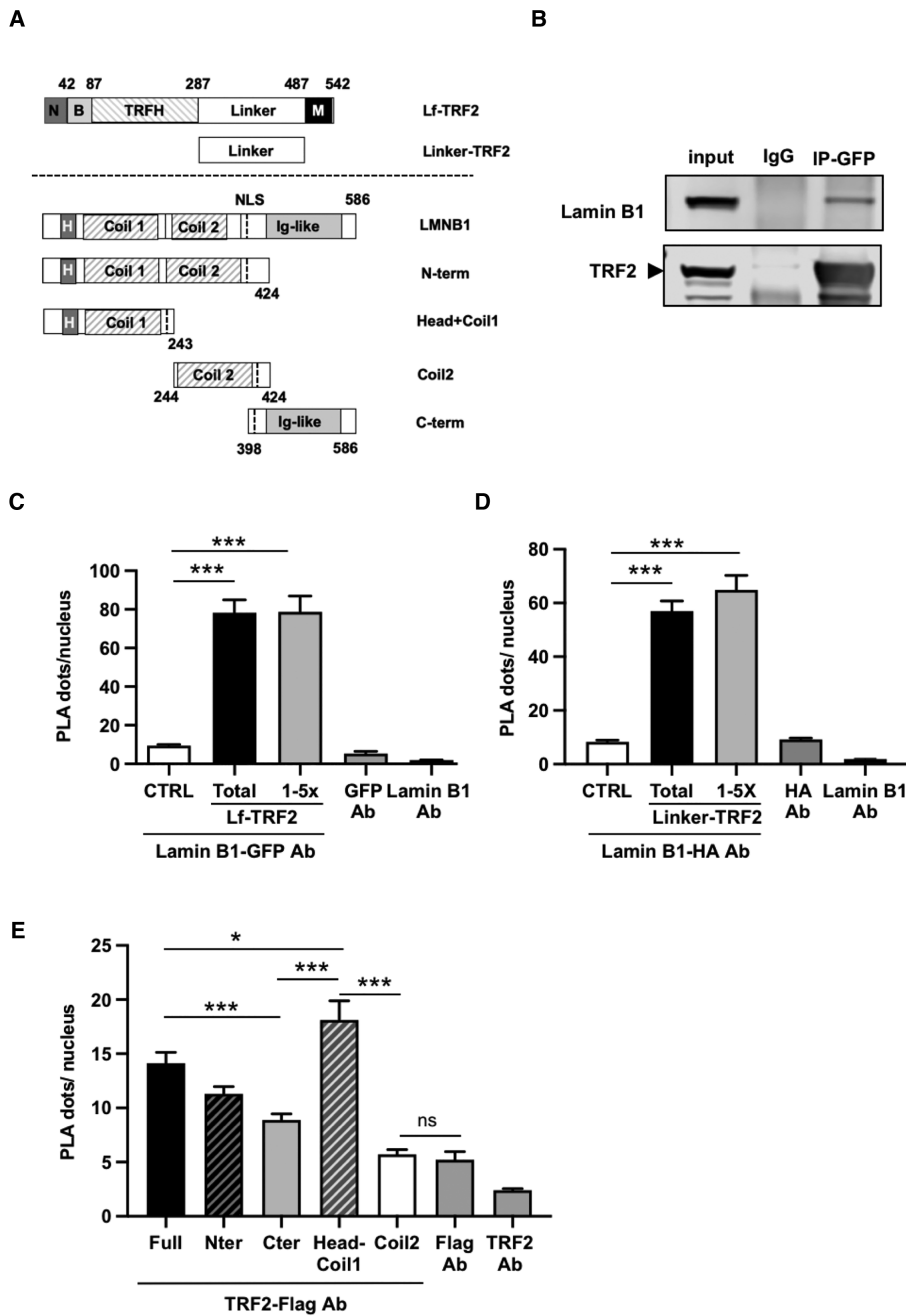


Figure 6. The Head-coil1 domain of lamin B1 and the linker region of TRF2 are involved in Lamin B1-TRF2 interaction. **(A)** Schematic illustration of TRF2 and Lamin B1 constructs used in PLA or co-IP experiments. For TRF2 constructs: Lf = long isoform, N = N-terminal domain, B = basic domain, TRFH = TRF Homology domain and Myb = DNA-binding domain. For lamin B1 constructs: H = head domain, NLS = nuclear localization signal; Coil = coiled-coil domain, Ig-fold = Immunoglobulin-like fold. **(B)** Endogenous lamin B1 interacts with the long form of TRF2: **(B)** pull-down with antibody against GFP or IgG, as control, were performed on protein lysates (pretreated with benzonase) from cells transfected with an expression plasmid of the long TRF2 isoform tagged with GFP. Arrow-head points band corresponding to GFP-TRF2; similar results were observed in two independent experiments. **(C)** PLA between endogenous lamin B1 and the long isoform of TRF2. PLA was performed with a specific antibody against lamin B1 and GFP in cells transfected as described above. Quantification of PLA dots per nuclei is shown in total or 1–5-fold (1–5×) overexpressing GFP-TRF2 long isoform (Lf-TRF2) (means per nuclei ± SEM from PLA spots were counted from a pool of two independent experiments; $n = 99$ and 194 nuclei; *** $P < 0.0001$). Negative PLA controls performed with one of the primary antibody against GFP or lamin B1 protein alone (GFP Ab or Lamin B1 Ab) are shown. **(D)** PLA between endogenous lamin B1 and the TRF2 linker domain. PLA was performed using specific antibodies against lamin B1 and HA tag in cells transfected with HA-TRF2 linker construct. Quantification of PLA dots per nuclei is shown in total or 1–5-fold (1–5×) overexpressing TRF2-linker domain (Linker-TRF2) (means ± SEM from three experiments are shown; *** $P < 0.0001$). Negative PLA controls performed with HA antibody alone (HA Ab) or lamin B1 (Lamin B1 Ab) are shown. **(E)** PLA between endogenous TRF2 and different lamin B1 domains. PLA was performed with specific antibodies against lamin B1 and Flag tag in cells transfected with the different Flag-lamin B1 constructs. For comparison between the different lamin B1 constructs, analysis is made among populations with similar Flag expression intensity for each construct. Quantification of PLA dots per nuclei is shown (means ± SEM from two experiments are shown; *** $P < 0.0001$). Negative PLA controls performed with Flag antibody alone (Flag Ab) or TRF2 (TRF2 Ab) are shown.

fected with the N-terminal part (1–424 aa) and more precisely the head-coil1 (1–243 aa) of lamin B1, as shown by the increase in PLA dots compared to control cells, while the coil2 (244–424 aa) and C-terminal domain (398–586 aa) of lamin B1 exhibited significantly a lower number of PLA dots (Figure 6E). These data indicate that the head-coil1 region of lamin B1 and the linker region of TRF2 are likely to be the domains responsible for the interaction between lamin B1 and TRF2.

Elevation of TRF2 level rescues telomere fusions induced by lamin B1 overexpression

Given that lamin B1 overexpression leads to an increased interaction with TRF2 at the nuclear periphery, in association with an apparent delocalization of this shelterin protein from telomeres and, at later time, an induction of telomeric aberrations, these results suggest that the capping function of TRF2 is impaired. We therefore hypothesize that lamin B1 in excess may sequester TRF2 preferentially at the nuclear periphery, thereby impairing its telomere capping function and subsequently leading to telomere instability. In order to identify whether telomeric instability is linked to an impairment of TRF2 function by lamin B1, we increased TRF2 protein levels in cells overexpressing lamin B1 and analyzed if the telomeric phenotype could be rescued. Thus, we performed complementation experiments by means of transitory transfections with an expression plasmid of TRF2 in immortalized fibroblasts overexpressing or not lamin B1. Expression levels of TRF2 and lamin B1 were checked by western-blots and comparable levels of lamin B1 proteins were detected in single-transfection with lamin B1 and double-transfection with both lamin B1 and TRF2 vectors (Figure 7A). In addition, by immunostaining, we observed that the percentage of cells overexpressing lamin B1 or TRF2 between single and double-transfection were similar, and that, in double-transfection conditions, almost all transfected cells were overexpressing both lamin B1 and TRF2 (Figure 7B), thereby allowing comparisons hereafter. We next analyzed the impact of TRF2 upregulation on lamin B1-induced chromosomal end-to-end fusions on metaphase spreads. Importantly, the mitotic index was similar between all conditions (Figure 7C), ruling out that cells with damages couldn't reach metaphase step in co-transfection condition. We found that the level of chromosome- and chromatid-type fusions in metaphases from cells overexpressing both lamin B1 and TRF2 (Figure 7D) was reduced to that observed in control cells ($9.9\% \pm 1.6$ and $8.8\% \pm 1.7$, respectively, with a t-test p value non-significant between the two conditions) while the level of telomeric aberrations was significantly increased in cells overexpressing lamin B1 alone ($24.0\% \pm 2.6$, $P < 0.0001$). Furthermore, we found that lamin B1-induced TIFs were significantly reduced by increasing the level of TRF2 (Figure 7E). These data indicate that increased level of TRF2 could rescue lamin B1-induced telomere instability, suggesting that additional TRF2 can titrate excessive lamin B1 interaction and allow TRF2 to protect again telomeres, and thereby to prevent telomeric fusions.

DISCUSSION

In this study, we investigate the link existing between the lamin B1 and telomeres and especially the consequences of lamin B1 increase on telomere stability. We showed that lamin B1 overexpression leads to telomere instability (i.e. TIFs induction, telomeric fusions and losses) and give some insights into the mechanism by which increased lamin B1 level affects telomeres (Figure 8). We unveil new interactions between lamin B1 and both TRF2 and RAP1, localized throughout the nucleoplasm in endogenous conditions. These interactions are dramatically enhanced at the nuclear periphery upon lamin B1 overexpression. We showed that the association between lamin B1 and TRF2 implicates the head-coil1 domain of lamin B1 and the flexible hinge region (or linker) of TRF2, a region implicated in protein-protein interactions, including binding with RAP1 (4,8,76) and that both shelterin proteins are required to form stable complexes with lamin B1. It has been reported that the linker of TRF2 presents structural similarities with rod domains of intermediate filaments (77) and is involved in DNA-specific oligomerization of TRF2 (78). Likewise, the head-coil1 domain of lamin B1, contains coiled-coil motifs also involved in lamin oligomerization. Thus, these data are in agreement with a potential physical association between the TRF2 linker region and the head-coil1 region of lamin B1. In addition, we show that both shelterin proteins, TRF2 and RAP1, are required to form stable complexes with lamin B1.

It was previously proposed that sequestration of protein at the nuclear envelope could inhibit their function (79). Upon lamin B1 overexpression, we found that interactions between lamin B1 and both TRF2 and RAP1 were strongly increased and relocalized preferentially at the nuclear envelope, while another main telomeric protein TRF1 was not affected. TRF2 binds preferentially to the telomeric DNA at the junction between double-strand telomeric DNA and single-strand 3'overhang (5), whereas TRF1 has been reported to bind all along the telomere tracts (80) and to have a higher binding affinity for telomeric DNA compared to TRF2 (81). Thus, the mislocalizations of TRF2 and RAP1 in cells overexpressing lamin B1, suggest that lamin B1 may alter the capping function of telomere by the sequestration of shelterin factors at the nuclear lamina, thereby leading to telomeric instability.

Dissociation of TRF2 from telomeres has been previously observed in different situations. Among them, expression of the dominant negative form of TRF2 (TRF2^{ΔBΔM}) leads to a diffuse nuclear staining pattern of TRF2. This mutant form lacking both the basic and the Myb DNA-binding domain can no longer bind telomeric DNA but can still make homodimer with endogenous TRF2. As stable binding of TRF2 homodimers on telomeric DNA requires two Myb domains, TRF2^{ΔBΔM} interferes with the accumulation of endogenous TRF2 protein at telomeres in a dominant-negative fashion (13). Consequently, telomeres are deprotected, recognized as DNA-damage (presence of TIFs) and are subjected to end-to-end chromosomal fusions (10,82). Depending on the cellular context, telomere dysfunction triggered by TRF2^{ΔBΔM} leads to reduced cell proliferation, senescence and cell death in p53-proficient

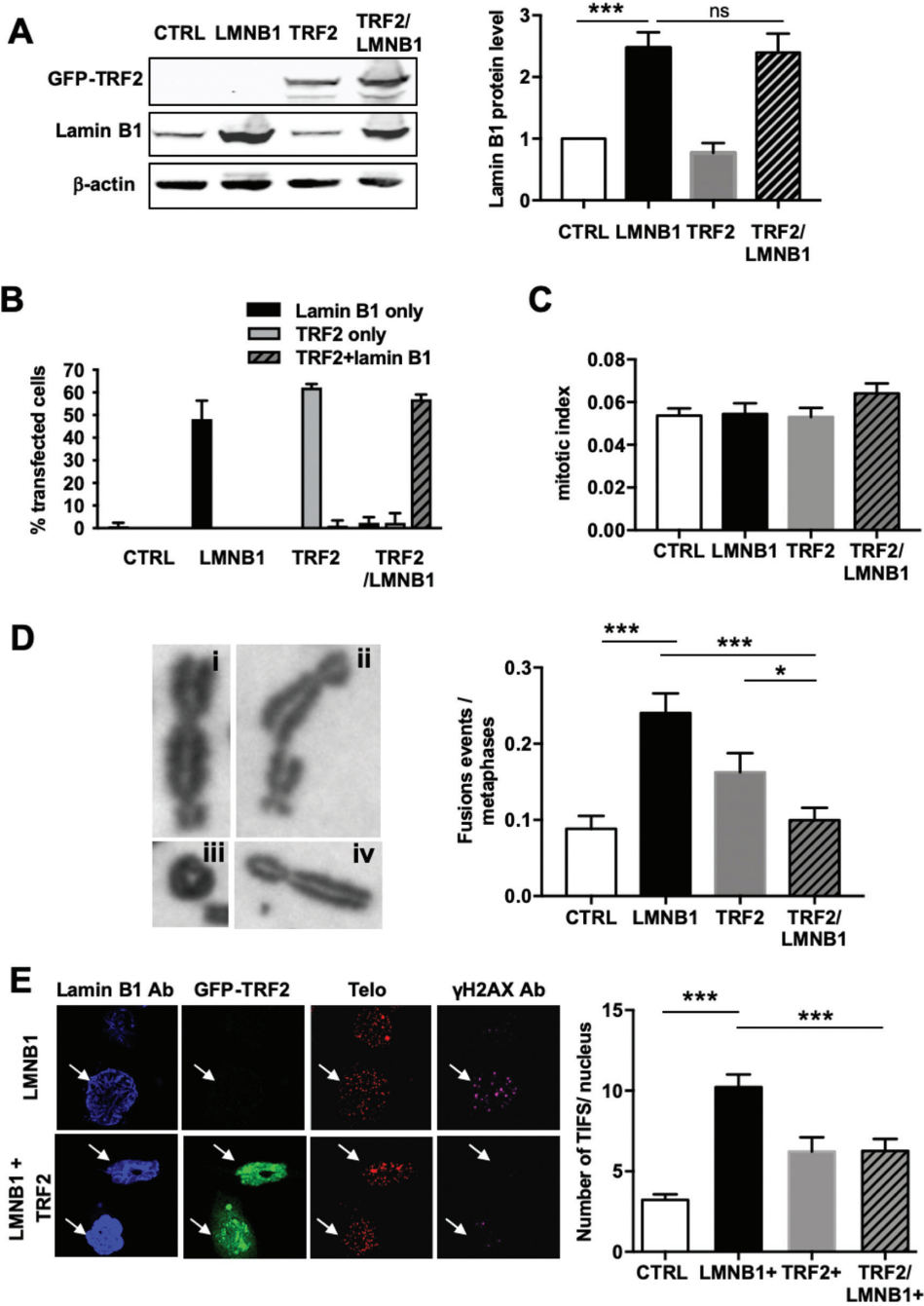


Figure 7. Elevation of TRF2 level rescues TIFs and end-to-end chromosome fusions induced by lamin B1 overexpression. (A) SV40-fibroblasts were transfected either with LMNB1 or GFP-TRF2 or CTRL vectors or co-transfected with both GFP-TRF2 and LMNB1 vectors. 48 h after transfections, GFP-TRF2- and lamin B1 protein levels were measured by western blots using specific antibodies to GFP, lamin B1 and β -actin. Histograms show the quantification of each protein level relative to β -actin (means \pm SEM of three independent experiments; *** $P = 0.0006$; ns = non-significant). (B) Quantification of the percentage of transfected cells in rescue experiments as described in (A) (mean \pm SD from 3 independent experiments; $n = 300\text{--}496$ cells analyzed per conditions). (C) Metaphase spreads were prepared from cells transfected as described in (A), 72 h after transfection, and stained with Giemsa. Mitotic indices (mean numbers of mitosis per 1000 cells \pm SEM, calculated from randomly selected fields, from three independent experiments ($n > 1000$ cells counted for each experiments)) in the different conditions of transfection are shown. (D) Chromosomal fusion events (including dicentrics, rings, chromatid-type fusions and sister chromatid fusions) were analyzed in metaphase spreads described in (B). Histogram shows the mean number of fusion events per metaphase (means \pm SEM of three independent experiments; $n \geq 303$ metaphases per conditions). Examples of typical chromosomal fusion events stained with Giemsa found during the experiments: dicentrics (i), rings (ii), chromatid-type fusions (iii) and sister chromatid fusion (iv), are shown in the right panel. (E) Immuno-FISH performed with antibodies to γ -H2AX (magenta) and lamin B1 (blue) and with a specific telomere PNA probe (red) on SV40-fibroblasts 48 h after transfection as described in (A). Cells with TRF2 overexpression were detected thanks to the GFP-tag (green). Representative images are shown. Arrows pointed double-transfected cells with lamin B1 and TRF2 overexpression showing reduced TIFs (γ -H2AX-telomere co-localizations). Histogram shows the number of TIFs (γ -H2AX foci colocalized at telomeres) per nucleus from control cells (CTRL), lamin B1- or TRF2-overexpressing cells (LMNB1+ or TRF2+), and cells co-overexpressing TRF2 and lamin B1 (TRF2+/LMNB1+) (mean \pm SEM of 3 independent experiments; $n > 50$ cells analyzed per conditions; *** t -test P values < 0.0001).

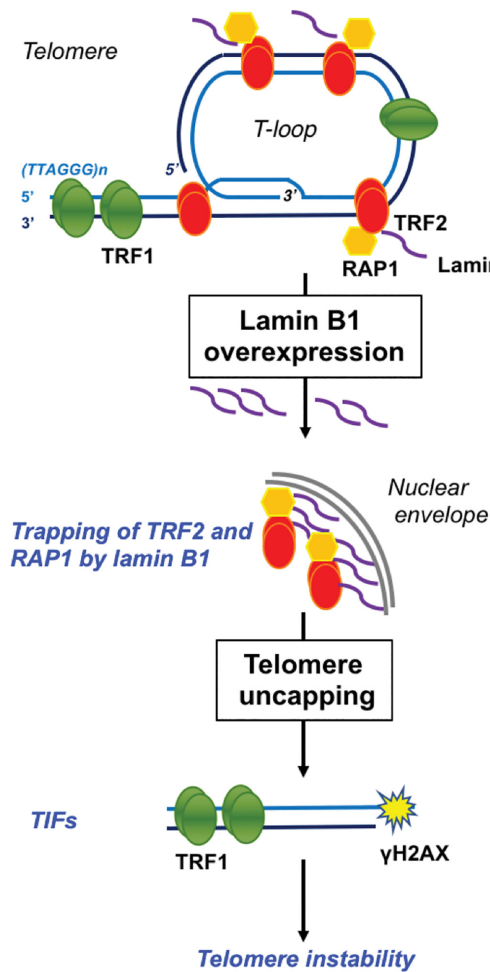


Figure 8. Model for lamin B1 overexpression-induced telomere instability in human cells. Lamin B1 overexpression leads to the mislocalization of the shelterin protein TRF2 and its binding partner RAP1 through enhanced interactions preferentially located at the nuclear periphery. Mislocalization of TRF2 and RAP1 could lead to telomere uncapping. Deprotected telomeres become recognized as damage by the DNA repair machinery (as assessed by the observation of TIFs). They could therefore undergo inappropriate repairs resulting in telomere instability marked by the observed telomeric fusions and telomere losses.

cells or genomic instability in p53-deficient cells (11,82). We and others previously showed that lamin B1 overexpression can lead to senescence in primary fibroblasts (42,52,62). We reported here that lamin B1 overexpression also induces telomeric instability (TIFs, end-to-end chromosomal fusions), phenotype reminiscent to that caused by TRF2 dysfunction. We showed that elevation of TRF2 protein level in cells overexpressing lamin B1 rescues the telomeric phenotype. Thus, the ectopic expression of TRF2 could compensate its delocalization from telomere by restoring a protective cap to telomeres thereby preventing end-to-end fusions of chromosomes. These results sustain our presumption that lamin B1 overexpression could impair TRF2 capping function by sequestration of this protein.

Links between telomere and lamins were previously reported, mainly for lamin A/C (83,84). Indeed, telomere attrition were observed in cells from HGPS patients due to

a mutation in lamin A gene that leads to an accumulation of progerin a mutant form of lamin A (68–70). This was also observed in progerin-expressing human fibroblasts (85). Furthermore, lamin A-deficient mouse cells exhibit also telomere shortening and alteration of telomere localizations (86). Although, involvement of lamin A/C deficiency in telomere dysfunction has been documented (83,84), the role of lamin B1 in telomere stability has been poorly explored. A previous study reported that proliferative defects from lamin B1-overexpressing cells are rescued by the telomerase catalytic subunit hTERT, suggesting that telomeric dysfunction could be involved in this phenotype (62). Thus, it was also critical to evaluate the impact of lamin B1 on telomere integrity. Beside sharing some similar functions regarding nuclear shape integrity and scaffolding protein function, lamin B1 and lamin A/C are not interchangeable lamins and have also distinct functions. Indeed, they form interconnected but separated networks (34,87,88), interact differentially with chromatin (89), and associate with common and distinct protein partners (90). Importantly, we noticed that lamin B1 dysregulation, overexpression did not impact the protein level of other lamins (A/C-type or B2 lamin) in western blot experiments. This data indicates that lamin B1-related impact on telomeres is not attributable to deficiency in other lamins, suggesting that telomere damages observed in our experiments are specifically induced by lamin B1 dysregulation. In our study, the delocalizations of TRF2 and RAP1 upon lamin B1 overexpression were not associated with a degradation of their protein levels. Unlike lamin B1, TRF2 degradation has been reported in fibroblasts from atypical Werner syndrome's patients carrying lamin A mutations (R133L and L140R) (91). In addition, Benson *et al.* reported that expression of progerin, the mutated form of lamin A deleted of 50 amino-acids involved in HGPS, induces TIFs as well as telomere aberrations, but did not cause a decreased association of TRF2 with telomeres (85), suggesting that progerin-induced TIFs do not result from dramatic loss of TRF2 binding to telomeres. These observations indicate that similarly, as for progerin, lamin B1 overexpression leads to TIFs and telomere instability, but, unlike progerin, TRF2 is delocalized from telomeres. Although alterations in any lamina component appears to impact telomere stability, the mechanisms of telomere dysfunction induced by progerin and lamin A mutations may differ from that caused by lamin B1 overexpression. Wood *et al.* reported that progerin does not interact with TRF2 protein in co-immunoprecipitation experiments, while a small fraction of the total TRF2 and wild-type lamin A/C can interact together (92). The different impact on TRF2 protein localization between progerin and lamin B1 may be in part explained by the lack of interaction between progerin and TRF2. Furthermore, lamin A/C and B1 were reported to have different *in vitro* binding properties with telomeres: lamin A/C binding to telomere sequences is quite more efficient than that of lamin B1 (31,73). Altogether, these observations indicate that although both lamin A/C and lamin B1 were found to play a role in telomere stability, they may have a differential role at telomere.

Almost 30 years ago, human telomeres were reported to be attached to the nuclear matrix (93). Later, it was reported

that telomeres are enriched at the nuclear periphery during post-mitotic nuclear assembly (29), as well as a subset of telomeres during replication (30). In addition, in cellular extracts from enriched post-mitotic EGFP-TRF1 transfected cells, an interaction between the telomeric protein TRF1 and lamin B1 was reported, but not in endogenous conditions (29). Moreover, an interaction between lamin A/C and TRF2 was found (92) although no direct interaction was established between lamins and telomeres. Recently contact of telomeres with nuclear envelope was also detected in G1/S arrested HeLa cells using MadID, an optimized approach for mapping protein-DNA interactions, suggesting that contact of telomere with the nuclear rim can as well occur outside of mitosis (94). Wood *et al.* propose a functional role of the TRF2-lamin A/C interaction. Indeed, they showed that TRF2 can form t-loops with interstitial telomeric sequences (ITL) which are stabilized by interaction with lamin A/C (92). They further suggest that these ITL structures are novel chromosome-end structures. Whether lamin B1 is also involved in the stabilization of the ITL, as previously proposed for lamin A (92), requires future investigations.

Beside its anchoring to the inner nuclear envelope (32), a pool of lamin B1 is also present in the nucleus and is forming stable structures (34,43,46). Considering these observations, lamin B1 may serve as an anchoring matrix for telomeric chromatin through its interaction with shelterin protein. Indeed, interacting dots between endogenous lamin B1 and TRF2 or RAP1 were found localized throughout the nucleus, and may correspond to sites of stable intranuclear structures of lamin B1, as previously described. Furthermore, colocalization of nuclear lamin B1 with sites of DNA replication and with PCNA have been reported (95). It was also reported that decrease in lamin B1 leads to defects in DNA replication (96), suggesting a role for lamin B1 in DNA replication. These studies prompt us to propose a second hypothesis, not exclusive, on the role of lamin B1 in telomere stability. Indeed, lamin B1 may be involved in telomere replication and/or in the regulation of TRF2. The binding of TRF2 to telomeres was previously reported to have a negative impact on the progression of replicative forks at the telomeric repeats tracts (97), suggesting that TRF2 has to be removed from telomere to enable its replication. Thus, lamin B1 could serve as a reservoir of TRF2 during replication that transiently delocalized TRF2 from telomere to enable t-loop resolution and further telomere replication. Recently, a phospho-site of TRF2 (S365), located in the linker domain, has been involved in the regulation of TRF2's interaction with helicase RTEL1 in S-phase to facilitate telomere replication. Indeed, dephosphorylation of TRF2 at S365 enables access of RTEL1 to telomere to unwind t-loop and facilitates telomere replication, while re-phosphorylation of TRF2 at S365 is required to prevent access of RTEL1 to telomeres thereby protecting telomeres from unwinding (98). Thus, the interaction between lamin B1 with TRF2 could also participate to the regulation of this phospho-switch.

Upon lamin B1 overexpression, we observed a significant increase in telomeric fusions and telomere losses. Telomere dysfunction that results in end-to-end chromosomal fusions can initiate breakage-fusion-bridge (B/F/B) cycles and has

usually dramatic impacts on genome stability leading to genomic rearrangements and changes in ploidy, thus affecting cancer development and progression (60,61). In accordance, lamin B1 overexpression has been reported in many cancer cell types and has been correlated with aggressiveness in different tumors (55,99), but how lamin B1 may participate to tumorigenesis is still unclear. Our data could give some insights about the impact of lamin B1 dysregulation on the genome of tumor cells. Indeed, considering our findings on the role of lamin B1 at telomere, we suggest that overexpression of lamin B1 may increase telomere dysfunction of cancer cells and thereby amplify chromosome instability in course of tumorigenesis.

In summary, our study has uncovered that lamin B1 overexpression leads to the sequestration of shelterin TRF2 and RAP1 proteins, mostly at the nuclear periphery, impeding their protective function at telomere and, thereby, resulting in telomere instability (Figure 8). Our data highlight the importance of lamin B1 regulation to maintain functional telomeres, and thereby genome integrity.

SUPPLEMENTARY DATA

[Supplementary Data](#) are available at NAR Online.

ACKNOWLEDGEMENTS

We would like to thank all members of the LREV lab for advice and support and especially Emilie Rass for the proofreading of the manuscript. We would also like to thank Denis Gomez (IPBS, France) for providing TRF2 vectors. We thank Xavier Veaute and Jordane Dépagnie (CiGEX platform) for their expertise on protein interactions, Florian Roisné-Hamelin (LTR, iRCM) for experimental advices and Elea Dizet (CiGEX platform, CEA) for plasmid constructions. We acknowledge Stéphane Marcaud (LTR, iRCM) and Karine Dubrana (LION, iRCM) for helpful discussions and their comments on the manuscript.

FUNDING

Ligue Nationale Contre le Cancer (Ile de France committee); Association for Research against Cancer (Foundation ARC); AT Europe Association; ‘Radiobiology program’ CEA grant; INCA grant; AFM grant; INSERM house funding; J.P. is a recipient of a PhD fellowship of the french Ministry of Higher Education Research and Innovation (MESRI) from the ED of Cancerology (Gustave Roussy-University Paris-Saclay); L.E. was supported by a Ligue Nationale Contre le Cancer fellowship (Haut-de-Seine committee); INSERM house funding; A-R.R. was a recipient of a fellowship from ERASMUS-Leonardo da Vinci program (Sapienza University, Roma); P.F-R. was recipient of a PhD fellowship from the ED SDSV (University Paris-Saclay); Ligue Nationale Contre le Cancer. Funding for open access charge: Commissariat à l’Energie Atomique et aux Energies Alternatives.

Conflict of interest statement. None declared.

REFERENCES

1. Cesare,A.J. and Karlseder,J. (2012) A three-state model of telomere control over human proliferative boundaries. *Curr. Opin. Cell Biol.*, **24**, 731–738.
2. de Lange,T. (2005) Shelterin: the protein complex that shapes and safeguards human telomeres. *Genes Dev.*, **19**, 2100–2110.
3. Bilaud,T., Brun,C., Ancelin,K., Koering,C.E., Laroche,T. and Gilson,E. (1997) Telomeric localization of TRF2, a novel human telobox protein. *Nat. Genet.*, **17**, 236–239.
4. Broccoli,D., Smogorzewska,A., Chong,L. and de Lange,T. (1997) Human telomeres contain two distinct Myb-related proteins, TRF1 and TRF2. *Nat. Genet.*, **17**, 231–235.
5. Stansel,R.M., de Lange,T. and Griffith,J.D. (2001) T-loop assembly in vitro involves binding of TRF2 near the 3' telomeric overhang. *EMBO J.*, **20**, 5532–5540.
6. Karlseder,J., Hoke,K., Mirzoeva,O.K., Bakkenist,C., Kastan,M.B., Petrini,J.H.J. and de Lange,T. (2004) The telomeric protein TRF2 binds the ATM kinase and can inhibit the ATM-dependent DNA damage response. *PLoS Biol.*, **2**, E240.
7. Denchi,E.L. and de Lange,T. (2007) Protection of telomeres through independent control of ATM and ATR by TRF2 and POT1. *Nature*, **448**, 1068–1071.
8. Okamoto,K., Bartocci,C., Ouzounov,I., Diedrich,J.K., Yates,J.R. and Denchi,E.L. (2013) A two-step mechanism for TRF2-mediated chromosome-end protection. *Nature*, **494**, 502–505.
9. Feuerhahn,S., Chen,L., Luke,B. and Porro,A. (2015) No DDRama at chromosome ends: TRF2 takes centre stage. *Trends Biochem. Sci.*, **40**, 275–285.
10. Takai,H., Smogorzewska,A. and de Lange,T. (2003) DNA damage foci at dysfunctional telomeres. *Curr. Biol.*, **13**, 1549–1556.
11. Karlseder,J., Broccoli,D., Dai,Y., Hardy,S. and de Lange,T. (1999) p53- and ATM-dependent apoptosis induced by telomeres lacking TRF2. *Science*, **283**, 1321–1325.
12. Smogorzewska,A. and de Lange,T. (2002) Different telomere damage signaling pathways in human and mouse cells. *EMBO J.*, **21**, 4338–4348.
13. van Steensel,B., Smogorzewska,A. and de Lange,T. (1998) TRF2 protects human telomeres from end-to-end fusions. *Cell*, **92**, 401–413.
14. Li,B., Oestreich,S. and de Lange,T. (2000) Identification of human Rap1: implications for telomere evolution. *Cell*, **101**, 471–483.
15. Janoušková,E., Nečasová,I., Pavloušková,J., Zimmermann,M., Hluchý,M., Marini,V., Nováková,M. and Hofr,C. (2015) Human Rap1 modulates TRF2 attraction to telomeric DNA. *Nucleic Acids Res.*, **43**, 2691–2700.
16. Sfeir,A., Kabir,S., van Overbeek,M., Celli,G.B. and de Lange,T. (2010) Loss of Rap1 induces telomere recombination in the absence of NHEJ or a DNA damage signal. *Science*, **327**, 1657–1661.
17. Rai,R., Chen,Y., Lei,M. and Chang,S. (2016) TRF2-RAP1 is required to protect telomeres from engaging in homologous recombination-mediated deletions and fusions. *Nat. Commun.*, **7**, 10881.
18. Bae,N.S. and Baumann,P. (2007) A RAP1/TRF2 complex inhibits nonhomologous end-joining at human telomeric DNA ends. *Mol. Cell*, **26**, 323–334.
19. Sarthy,J., Bae,N.S., Scrafford,J. and Baumann,P. (2009) Human RAP1 inhibits non-homologous end joining at telomeres. *EMBO J.*, **28**, 3390–3399.
20. Bombarde,O., Boby,C., Gomez,D., Frit,P., Giraud-Panis,M.-J., Gilson,E., Salles,B. and Calsou,P. (2010) TRF2/RAP1 and DNA-PK mediate a double protection against joining at telomeric ends. *EMBO J.*, **29**, 1573–1584.
21. Lototska,L., Yue,J.-X., Li,J., Giraud-Panis,M.-J., Songyang,Z., Royle,N.J., Liti,G., Ye,J., Gilson,E. and Mendez-Bermudez,A. (2020) Human RAP1 specifically protects telomeres of senescent cells from DNA damage. *EMBO Rep.*, **21**, e49076.
22. Shay,J.W. and Wright,W.E. (2019) Telomeres and telomerase: three decades of progress. *Nat. Rev. Genet.*, **20**, 299–309.
23. Cesare,A.J. and Reddel,R.R. (2010) Alternative lengthening of telomeres: models, mechanisms and implications. *Nat. Rev. Genet.*, **11**, 319–330.
24. Longhese,M.P. (2008) DNA damage response at functional and dysfunctional telomeres. *Genes Dev.*, **22**, 125–140.
25. Cicconi,A. and Chang,S. (2020) Shelterin and the replisome: at the intersection of telomere repair and replication. *Curr. Opin. Genet. Dev.*, **60**, 77–84.
26. Gilson,E., Laroche,T. and Gasser,S.M. (1993) Telomeres and the functional architecture of the nucleus. *Trends Cell Biol.*, **3**, 128–134.
27. Shibuya,H. and Watanabe,Y. (2014) The meiosis-specific modification of mammalian telomeres. *Cell Cycle Georget. Tex.*, **13**, 2024–2028.
28. Ludérus,M.E., van Steensel,B., Chong,L., Sibon,O.C., Cremers,F.F. and de Lange,T. (1996) Structure, subnuclear distribution, and nuclear matrix association of the mammalian telomeric complex. *J. Cell Biol.*, **135**, 867–881.
29. Crabbe,L., Cesare,A.J., Kasuboski,J.M., Fitzpatrick,J.A.J. and Karlseder,J. (2012) Human telomeres are tethered to the nuclear envelope during postmitotic nuclear assembly. *Cell Rep.*, **2**, 1521–1529.
30. Arnoult,N., Schluth-Bolard,C., Letessier,A., Drascovic,I., Bouarich-Bourimi,R., Campisi,J., Kim,S., Boussouar,A., Ottaviani,A., Magdinier,F. et al. (2010) Replication timing of human telomeres is chromosome arm-specific, influenced by subtelomeric structures and connected to nuclear localization. *PLoS Genet.*, **6**, e1000920.
31. Raz,V., Vermolen,B.J., Garini,Y., Onderwater,J.J.M., Mommaas-Kienhuis,M.A., Koster,A.J., Young,I.T., Tanke,H. and Dirks,R.W. (2008) The nuclear lamina promotes telomere aggregation and centromere peripheral localization during senescence of human mesenchymal stem cells. *J. Cell Sci.*, **121**, 4018–4028.
32. Dechat,T., Adam,S.A., Taimen,P., Shimi,T. and Goldman,R.D. (2010) Nuclear lamins. *Cold Spring Harb. Perspect. Biol.*, **2**, a000547.
33. de Leeuw,R., Gruenbaum,Y. and Medalia,O. (2018) Nuclear lamins: thin filaments with major functions. *Trends Cell Biol.*, **28**, 34–45.
34. Shimi,T., Pfleghaar,K., Kojima,S., Pack,C.-G., Solovei,I., Goldman,A.E., Adam,S.A., Shumaker,D.K., Kinjo,M., Cremer,T. et al. (2008) The A- and B-type nuclear lamin networks: microdomains involved in chromatin organization and transcription. *Genes Dev.*, **22**, 3409–3421.
35. Röber,R.A., Weber,K. and Osborn,M. (1989) Differential timing of nuclear lamin A/C expression in the various organs of the mouse embryo and the young animal: a developmental study. *Dev. Camb. Engl.*, **105**, 365–378.
36. Eriksson,M., Brown,W.T., Gordon,L.B., Glynn,M.W., Singer,J., Scott,L., Erdos,M.R., Robbins,C.M., Moses,T.Y., Berglund,P. et al. (2003) Recurrent de novo point mutations in lamin A cause Hutchinson-Gilford progeria syndrome. *Nature*, **423**, 293–298.
37. De Sandre-Giovannoli,A., Bernard,R., Cau,P., Navarro,C., Amiel,J., Boccaccio,I., Lyonnet,S., Stewart,C.L., Munnich,A., Le Merrer,M. et al. (2003) Lamin a truncation in Hutchinson-Gilford progeria. *Science*, **300**, 2055.
38. Burke,B. and Stewart,C.L. (2013) The nuclear lamins: flexibility in function. *Nat. Rev. Mol. Cell Biol.*, **14**, 13–24.
39. Schulze,S.R., Curio-Penny,B., Speese,S., Dialynas,G., Cryderman,D.E., McDonough,C.W., Nalbant,D., Petersen,M., Budnik,V., Geyer,P.K. et al. (2009) A comparative study of Drosophila and human A-type lamins. *PLoS One*, **4**, e7564.
40. Stewart,C. and Burke,B. (1987) Teratocarcinoma stem cells and early mouse embryos contain only a single major lamin polypeptide closely resembling lamin B. *Cell*, **51**, 383–392.
41. Freund,A., Laberge,R.-M., Demaria,M. and Campisi,J. (2012) Lamin B1 loss is a senescence-associated biomarker. *Mol. Biol. Cell*, **23**, 2066–2075.
42. Shimi,T., Butin-Israeli,V., Adam,S.A., Hamanaka,R.B., Goldman,A.E., Lucas,C.A., Shumaker,D.K., Kosak,S.T., Chandel,N.S. and Goldman,R.D. (2011) The role of nuclear lamin B1 in cell proliferation and senescence. *Genes Dev.*, **25**, 2579–2593.
43. Moir,R.D., Montag-Lowy,M. and Goldman,R.D. (1994) Dynamic properties of nuclear lamins: lamin B is associated with sites of DNA replication. *J. Cell Biol.*, **125**, 1201–1212.
44. Dechat,T., Gesson,K. and Foisner,R. (2010) Lamina-independent lamins in the nuclear interior serve important functions. *Cold Spring Harb. Symp. Quant. Biol.*, **75**, 533–543.
45. Shimi,T., Kittisopikul,M., Tran,J., Goldman,A.E., Adam,S.A., Zheng,Y., Jaqaman,K. and Goldman,R.D. (2015) Structural organization of nuclear lamins A, C, B1, and B2 revealed by superresolution microscopy. *Mol. Biol. Cell*, **26**, 4075–4086.

46. Naetar,N., Ferraioli,S. and Foisner,R. (2017) Lamins in the nuclear interior - life outside the lamina. *J. Cell Sci.*, **130**, 2087–2096.
47. Jia,Y., Vong,J.S.-L., Asafova,A., Garvalov,B.K., Caputo,L., Cordero,J., Singh,A., Boettger,T., Günther,S., Fink,L. *et al.* (2019) Lamin B1 loss promotes lung cancer development and metastasis by epigenetic derepression of RET. *J. Exp. Med.*, **216**, 1377–1395.
48. Cristofoli,F., Moss,T., Moore,H.W., Devriendt,K., Flanagan-Stet,H., May,M., Jones,J., Roelens,F., Fons,C., Fernandez,A. *et al.* (2020) De Novo Variants in LMNB1 cause pronounced syndromic microcephaly and disruption of nuclear envelope integrity. *Am. J. Hum. Genet.*, **107**, 753–762.
49. Parry,D.A., Martin,C.-A., Greene,P., Marsh,J.A. and Genomics England Research ConsortiumGenomics England Research Consortium, Blyth,M., Cox,H., Donnelly,D., Greenhalgh,L., Greville-Heygate,S. *et al.* (2021) Heterozygous lamin B1 and lamin B2 variants cause primary microcephaly and define a novel laminopathy. *Genet. Med. Off. J. Am. Coll. Med. Genet.*, **23**, 408–414.
50. Padiath,Q.S., Saigoh,K., Schiffmann,R., Asahara,H., Yamada,T., Koeppen,A., Hogan,K., Ptácek,L.J. and Fu,Y.-H. (2006) Lamin B1 duplications cause autosomal dominant leukodystrophy. *Nat. Genet.*, **38**, 1114–1123.
51. Donadille,B., D'Anella,P., Auclair,M., Uhrhammer,N., Sorel,M., Grigorescu,R., Ouzounian,S., Cambonie,G., Boulot,P., Laforêt,P. *et al.* (2013) Partial lipodystrophy with severe insulin resistance and adult progeria Werner syndrome. *Orphanet J. Rare Dis.*, **8**, 106.
52. Barascu,A., Le Chalony,C., Pennarun,G., Genet,D., Imam,N., Lopez,B. and Bertrand,P. (2012) Oxidative stress induces an ATM-independent senescence pathway through p38 MAPK-mediated lamin B1 accumulation. *EMBO J.*, **31**, 1080–1094.
53. Capo-chichi,C.D., Cai,K.Q., Simpkins,F., Ganjei-Azar,P., Godwin,A.K. and Xu,X.-X. (2011) Nuclear envelope structural defects cause chromosomal numerical instability and aneuploidy in ovarian cancer. *BMC Med.*, **9**, 28.
54. Coradeghini,R., Barbora,P., Rubagotti,A., Boccardo,F., Parodi,S., Carmignani,G., D'Arrigo,C., Patroni,E. and Balbi,C. (2006) Differential expression of nuclear lamins in normal and cancerous prostate tissues. *Oncol. Rep.*, **15**, 609–613.
55. Irianto,J., Pfeifer,C.R., Ivanovska,I.L., Swift,J. and Discher,D.E. (2016) Nuclear lamins in cancer. *Cell. Mol. Bioeng.*, **9**, 258–267.
56. Radspieler,M.M., Schindeldecker,M., Stenzel,P., Först,S., Tagscherer,K.E., Herpel,E., Hohenfellner,M., Hatiboglu,G., Roth,W. and Macher-Goeppinger,S. (2019) Lamin-B1 is a senescence-associated biomarker in clear-cell renal cell carcinoma. *Oncol. Lett.*, **18**, 2654–2660.
57. Li,L., Du,Y., Kong,X., Li,Z., Jia,Z., Cui,J., Gao,J., Wang,G. and Xie,K. (2013) Lamin B1 is a novel therapeutic target of betulinic acid in pancreatic cancer. *Clin. Cancer Res.*, **19**, 4651–4661.
58. Sun,S., Xu,M.Z., Poon,R.T., Day,P.J. and Luk,J.M. (2010) Circulating Lamin B1 (LMNB1) biomarker detects early stages of liver cancer in patients. *J. Proteome Res.*, **9**, 70–78.
59. Lv,D., Wu,X., Wang,M., Chen,W., Yang,S., Liu,Y., Zeng,G. and Gu,D. (2021) Functional assessment of four novel immune-related biomarkers in the pathogenesis of clear cell renal cell carcinoma. *Front. Cell Dev. Biol.*, **9**, 621618.
60. Murnane,J.P. and Sabatier,L. (2004) Chromosome rearrangements resulting from telomere dysfunction and their role in cancer. *BioEssays News Rev. Mol. Cell. Dev. Biol.*, **26**, 1164–1174.
61. Maciejowski,J. and de Lange,T. (2017) Telomeres in cancer: tumour suppression and genome instability. *Nat. Rev. Mol. Cell Biol.*, **18**, 175–186.
62. Dreesen,O., Chojnowski,A., Ong,P.F., Zhao,T.Y., Common,J.E., Lunny,D., Lane,E.B., Lee,S.J., Vardy,L.A., Stewart,C.L. *et al.* (2013) Lamin B1 fluctuations have differential effects on cellular proliferation and senescence. *J. Cell Biol.*, **200**, 605–617.
63. Etourneau,L., Moussa,A., Rass,E., Genet,D., Willaume,S., Chabance-Okumura,C., Wanshoor,P., Picotto,J., Thézé,B., Dépagnie,J. *et al.* (2021) Lamin B1 sequesters 53BP1 to control the recruitment of 53BP1 to DNA damage. *Sci. Adv.*, **7**, eabb3799.
64. Hayakawa,T., Zhang,F., Hayakawa,N., Ohtani,Y., Shinmyozu,K., Nakayama,J. and Andreassen,P.R. (2010) MRG15 binds directly to PALB2 and stimulates homology-directed repair of chromosomal breaks. *J. Cell Sci.*, **123**, 1124–1130.
65. Cesare,A.J., Heaphy,C.M. and O'Sullivan,R.J. (2015) Visualization of telomere integrity and function in vitro and in vivo using immunofluorescence techniques. *Curr. Protoc. Cytom.*, **73**, 12.40.1–12.40.31.
66. Schuster,J., Sundblom,J., Thuresson,A.-C., Hassin-Baer,S., Klopstock,T., Dichgans,M., Cohen,O.S., Raininko,R., Melberg,A. and Dahl,N. (2011) Genomic duplications mediate overexpression of lamin B1 in adult-onset autosomal dominant leukodystrophy (ADLD) with autonomic symptoms. *Neurogenetics*, **12**, 65–72.
67. Giorgio,E., Rolyan,H., Kropp,L., Chakka,A.B., Yatsenko,S., Di Gregorio,E., Lacerenza,D., Vaula,G., Talarico,F., Mandich,P. *et al.* (2013) Analysis of LMNB1 duplications in autosomal dominant leukodystrophy provides insights into duplication mechanisms and allele-specific expression. *Hum. Mutat.*, **34**, 1160–1171.
68. Allsopp,R.C., Vaziri,H., Patterson,C., Goldstein,S., Younglai,E.V., Futcher,A.B., Greider,C.W. and Harley,C.B. (1992) Telomere length predicts replicative capacity of human fibroblasts. *Proc. Natl. Acad. Sci. U.S.A.*, **89**, 10114–10118.
69. Decker,M.L., Chavez,E., Vulto,I. and Lansdorp,P.M. (2009) Telomere length in Hutchinson-Gilford progeria syndrome. *Mech. Ageing Dev.*, **130**, 377–383.
70. Huang,S., Risques,R.A., Martin,G.M., Rabinovitch,P.S. and Oshima,J. (2008) Accelerated telomere shortening and replicative senescence in human fibroblasts overexpressing mutant and wild-type lamin A. *Exp. Cell Res.*, **314**, 82–91.
71. Harrington,L. and Robinson,M.O. (2002) Telomere dysfunction: multiple paths to the same end. *Oncogene*, **21**, 592–597.
72. Yorifuji,H., Tadano,Y., Tsuchiya,Y., Ogawa,M., Goto,K., Umetani,A., Asaka,Y. and Arahata,K. (1997) Emerin, deficiency of which causes Emery-Dreifuss muscular dystrophy, is localized at the inner nuclear membrane. *Neurogenetics*, **1**, 135–140.
73. Shoeman,R.L. and Traub,P. (1990) The in vitro DNA-binding properties of purified nuclear lamin proteins and vimentin. *J. Biol. Chem.*, **265**, 9055–9061.
74. Timashev,L.A. and de Lange,T. (2020) Characterization of t-loop formation by TRF2. *Nucl. Austin Tex.*, **11**, 164–177.
75. Travina,A.O., Illicheva,N.V., Mittenberg,A.G., Shabelnikov,S.V., Kotova,A.V. and Podgornaya,O.I. (2021) The long linker region of telomere-binding protein TRF2 is responsible for interactions with lamins. *Int. J. Mol. Sci.*, **22**, 3293.
76. Chen,Y., Rai,R., Zhou,Z.-R., Kanoh,J., Ribeyre,C., Yang,Y., Zheng,H., Damay,P., Wang,F., Tsujii,H. *et al.* (2011) A conserved motif within RAP1 has diversified roles in telomere protection and regulation in different organisms. *Nat. Struct. Mol. Biol.*, **18**, 213–221.
77. Illicheva,N.V., Podgornaya,O.I. and Voronin,A.P. (2015) Telomere repeat-binding factor 2 is responsible for the telomere attachment to the nuclear membrane. *Adv. Protein Chem. Struct. Biol.*, **101**, 67–96.
78. Khan,S.J., Yanez,G., Seldeen,K., Wang,H., Lindsay,S.M. and Fletcher,T.M. (2007) Interactions of TRF2 with model telomeric ends. *Biochem. Biophys. Res. Commun.*, **363**, 44–50.
79. Serebryannyy,L. and Misteli,T. (2018) Protein sequestration at the nuclear periphery as a potential regulatory mechanism in premature aging. *J. Cell Biol.*, **217**, 21–37.
80. Griffith,J., Bianchi,A. and de Lange,T. (1998) TRF1 promotes parallel pairing of telomeric tracts in vitro. *J. Mol. Biol.*, **278**, 79–88.
81. Hanaoka,S., Nagadoi,A. and Nishimura,Y. (2005) Comparison between TRF2 and TRF1 of their telomeric DNA-bound structures and DNA-binding activities. *Protein Sci. Publ. Protein Soc.*, **14**, 119–130.
82. Smogorzewska,A., Karlseder,J., Holtgreve-Grez,H., Jauch,A. and de Lange,T. (2002) DNA ligase IV-dependent NHEJ of deprotected mammalian telomeres in G1 and G2. *Curr. Biol. CB*, **12**, 1635–1644.
83. Burla,R., La Torre,M. and Saggio,I. (2016) Mammalian telomeres and their partnership with lamins. *Nucl. Austin Tex.*, **7**, 187–202.
84. Gonzalo,S. and Eissenberg,J.C. (2016) Tying up loose ends: telomeres, genomic instability and lamins. *Curr. Opin. Genet. Dev.*, **37**, 109–118.
85. Benson,E.K., Lee,S.W. and Aaronson,S.A. (2010) Role of progerin-induced telomere dysfunction in HGPS premature cellular senescence. *J. Cell Sci.*, **123**, 2605–2612.
86. Gonzalez-Suarez,I., Redwood,A.B., Perkins,S.M., Vermolen,B., Lichtenstejin,D., Grotsky,D.A., Morgado-Palacin,L., Gapud,E.J., Sleckman,B.P., Sullivan,T. *et al.* (2009) Novel roles for A-type lamins in telomere biology and the DNA damage response pathway. *EMBO J.*, **28**, 2414–2427.
87. Xie,W., Chojnowski,A., Boudier,T., Lim,J.S.Y., Ahmed,S., Ser,Z., Stewart,C. and Burke,B. (2016) A-type lamins form distinct

- filamentous networks with differential nuclear pore complex associations. *Curr. Biol. CB*, **26**, 2651–2658.
88. Nmezi,B., Xu,J., Fu,R., Armiger,T.J., Rodriguez-Bey,G., Powell,J.S., Ma,H., Sullivan,M., Tu,Y., Chen,N.Y. *et al.* (2019) Concentric organization of A- and B-type lamins predicts their distinct roles in the spatial organization and stability of the nuclear lamina. *Proc. Natl. Acad. Sci. U.S.A.*, **116**, 4307–4315.
89. Gesson,K., Rescheneder,P., Skoruppa,M.P., Haeseler,A., Dechat,T. and Foisner,R. (2016) A-type lamins bind both hetero- and euchromatin, the latter being regulated by lamina-associated polypeptide 2 alpha. *Genome Res.*, **26**, 462–473.
90. Dittmer,T.A., Sahni,N., Kubben,N., Hill,D.E., Vidal,M., Burgess,R.C., Roukos,V. and Misteli,T. (2014) Systematic identification of pathological lamin A interactors. *Mol. Biol. Cell*, **25**, 1493–1510.
91. Saha,B., Zitnik,G., Johnson,S., Nguyen,Q., Risques,R.A., Martin,G.M. and Oshima,J. (2013) DNA damage accumulation and TRF2 degradation in atypical Werner syndrome fibroblasts with LMNA mutations. *Front. Genet.*, **4**, 129.
92. Wood,A.M., Rendtlew Danielsen,J.M., Lucas,C.A., Rice,E.L., Scalzo,D., Shimi,T., Goldman,R.D., Smith,E.D., Le Beau,M.M. and Kosak,S.T. (2014) TRF2 and lamin A/C interact to facilitate the functional organization of chromosome ends. *Nat. Commun.*, **5**, 5467.
93. de Lange,T. (1992) Human telomeres are attached to the nuclear matrix. *EMBO J.*, **11**, 717–724.
94. Sobecki,M., Souaid,C., Boulay,J., Guérineau,V., Noordermeer,D. and Crabbe,L. (2018) MadID, a versatile approach to map protein-DNA interactions, highlights telomere-nuclear envelope contact sites in human cells. *Cell Rep.*, **25**, 2891–2903.
95. Shumaker,D.K., Solimando,L., Sengupta,K., Shimi,T., Adam,S.A., Grunwald,A., Strelkov,S.V., Aebi,U., Cardoso,M.C. and Goldman,R.D. (2008) The highly conserved nuclear lamin Ig-fold binds to PCNA: its role in DNA replication. *J. Cell Biol.*, **181**, 269–280.
96. Butin-Israeli,V., Adam,S.A., Jain,N., Otte,G.L., Neems,D., Wiesmüller,L., Berger,S.L. and Goldman,R.D. (2015) Role of lamin b1 in chromatin instability. *Mol. Cell. Biol.*, **35**, 884–898.
97. Ohki,R. and Ishikawa,F. (2004) Telomere-bound TRF1 and TRF2 stall the replication fork at telomeric repeats. *Nucleic Acids Res.*, **32**, 1627–1637.
98. Sarek,G., Kotsantis,P., Ruis,P., Van Ly,D., Margalef,P., Borel,V., Zheng,X.-F., Flynn,H.R., Snijders,A.F., Chowdhury,D. *et al.* (2019) CDK phosphorylation of TRF2 controls t-loop dynamics during the cell cycle. *Nature*, **575**, 523–527.
99. Sakthivel,K.M. and Sehgal,P. (2016) A novel role of lamins from genetic disease to cancer biomarkers. *Oncol. Rev.*, **10**, 309.